
Otto-von-Guericke University Magdeburg



Department of Computer Science
Faculty of Informatics

Master's Thesis

Heartbeat Driven Dynamical Liver Movement Analysis - Feasibility of a fibrosis staging method

Author:

Khamar Uz Zama Mohammed

October 18, 2021

Advisors:

Supervisor Prof. Dr. Christian Hansen	Supervisor Dr. Alfredo Illanes
Faculty of Informatics Otto-von-Guericke University Universitätsplatz 2 39106 Magdeburg, Germany	Faculty of Medicine Otto-von-Guericke University Universitätsplatz 2 39106 Magdeburg, Germany

Mohammed, Khamar Uz Zama:
*Heartbeat Driven Dynamical Liver Movement Analysis - Feasibility of a fibrosis
staging method*
Master's Thesis, Otto-von-Guericke University
Magdeburg, 2021.

Dedicated to those who inspired me to write,

and will not read it.

Declaration of Academic Integrity

I hereby declare that I have written the present work myself and did not use any sources or tools other than the ones indicated.

Date:
(Signature)

Acknowledgement

I would like to express sincere gratitude to my supervisor, Dr. Alfredo Illanes, for his continuous guidance and insightful comments that encouraged me to work with dedication.

I also would like to thank Prof. Dr. Christian Hansen for giving me this opportunity to do my thesis in his chair.

Special thanks to Dr. Jens Ziegler and INKA team members for their support, valuable input and suggestions during the development of this work.

Last but not least, I also would like to thank my family and friends for their continuous support and encouragement throughout my journey to the Master's degree.

Contents

Abstract

1 Introduction

1.1 Motivation	1
1.2 Research Questions	2
1.3 Structure of work	2

2 Liver fibrosis and state of the art

2.1 Liver Fibrosis	3
2.2 Diagnostic methods of liver fibrosis	4
2.3 State of the art in Research	8

3 Background

3.1 Deep Learning	15
3.1.1 Types of Learning	16
3.1.2 Image Segmentation	17
3.1.3 Metrics for Image Segmentation	18
3.1.4 U-Net for Image Segmentation	19
3.1.5 Layers	20
3.1.6 Activation Functions	20
3.1.7 Loss Functions	23
3.2 Optical Flow	25
3.2.1 Optical Flow with an example	26

4 Materials and Methods

4.1 Data Acquisition	30
4.2 Liver Segmentation	30
4.2.1 Preparing the dataset	32
4.2.2 Training segmentation model	33
4.3 Liver Movement Assessment	35
4.3.1 Location of Initial Observers	35
4.3.2 Estimation of Liver's Movement Trajectory	38
4.3.3 Computation of Intensity	40
4.4 Evaluation Procedure	40

5 Results

5.1 Liver Movement Analysis	45
5.2 Multi-Liver Correlation Analysis	51

6 Discussion**7 Future Work****8 Conclusion****A Abbreviations and Notations****B List of Figures****C List of Tables****D Bibliography**

Abstract

Diseases linked to fibrosis pose an extensive health problem due to its heterogeneity and diverse causes. Studies estimate that cirrhosis, which is the late stage of fibrosis is responsible for almost 1.3 million deaths. The term fibrosis refers to the formation of scar tissue accumulated on the walls or vessels of organs which interfere with the normal functioning of the underlying organ. Liver fibrosis occurs in stages from F0 (normal) - F4 (cirrhosis), with F4 stage being fatal. As the liver fibrosis disease worsens from F0 to F4, there is accumulation of scar tissue deposits which make the liver stiff. The current widely used elastography methods diagnose liver fibrosis indirectly by measuring the liver stiffness with advanced equipment and special probes for excitation. They are expensive and they also have certain limitations like dependency on operator's skill and intra/inter observer variance.

The aim of this thesis is to explore if there is a relation between liver's movement and it's fibrotic stage using only heartbeat as the mechanism for internal excitation. A positive answer to this question would make the diagnosis of liver fibrosis inexpensive and accessible by minimizing the use of advanced equipment and ultrasound probes. In this thesis ultrasound scans are used as imaging source and heartbeat is used as internal excitation mechanism. Due to close proximity of liver to the heart, each heartbeat causes an excitation to the liver at the region of excitation. The underlying assumption of this research is that a normal liver, which is soft, would absorb the energy from internal excitation better than a hard fibrotic liver. As the distance from the region of excitation increases, there is decrease in the energy. This is called damping. Thus, from the assumption, healthy livers are expected to have higher damping from the heart's excitation than fibrotic livers. To compute this damping, firstly, the region of interest i.e. liver is identified using supervised deep learning methods. Using the identified liver boundaries and optical flow methods, the behavior of liver's movement is tracked by placing multiple so called *Observers*. These *Observers* track the magnitude and direction of liver's movement due to heart's excitation. In this work, 15 ultrasound scans along with their FibroScan test results are analyzed to observe the damping across the liver starting from the region of excitation. The average mean damping of the F0/F1, F2, F3 and F4 fibrotic stage livers is observed to be 69%, 80%, 77% and 88% respectively. The results have shown that there is high damping in early fibrosis stages when compared to late fibrosis stages.

1

Introduction

1.1 Motivation

Liver is the second largest organ of our body after skin and it performs over 500 vital functions. Its main function is to purify the blood by breaking down the toxic substances while regulating sugar levels of blood and creating essential enzymes like bile and amino acids [1].

According to the study conducted by Tapper et al. [2], from 1999 to 2016, the annual deaths due to cirrhosis, increased by 65% to 34,174 in United States alone. Alcohol abuse and viral infections are the leading causes of cirrhosis. A study on global alcohol consumption [3] concluded that there is 70% increase in alcohol consumption from 1990 to 2017 and it is expected to continue this trend in future. Due to asymptomatic nature of disease, it is rarely diagnosed in its early stages. Presently, elastography and imaging techniques are widely used non-invasive methods to detect fibrosis. Not only they are expensive they also require additional set-ups for external excitation mechanism to measure liver stiffness. These techniques have certain limitations like high dependency on operator's skill and intra/inter observer variance [4] while discrepancies due to probe placement have also been observed in ultrasound diagnostics [5].

The above cited reasons and a strong hypothesis that a healthy liver which is soft would absorb the heart's excitation better than a hard fibrotic liver serve as motivation for this work. In this work optical flow and deep learning methods are used with heart as internal excitation mechanism to check if liver's movement can be associated with its fibrosis stage.

1.2 Research Questions

This thesis mainly focuses on exploring solutions for the following research questions:

- Is optical flow combined with deep learning methods suitable to relate liver's movement with it's fibrosis stage?
- Is it possible to estimate liver's fibrosis stage using only ultrasound scans?
- Can the use of advanced hardware be minimized in detecting liver fibrosis?

1.3 Structure of work

- Chapter 2 gives a brief introduction to liver fibrosis, its causes and stages. It also covers the current state of the art methods in diagnosing liver fibrosis in applied medicine and research.
- Chapter 3 explains the background knowledge of technical concepts on deep learning and optical flow.
- Chapter 4 illustrates the methods conducted to answer the research questions and also their evaluation procedure.
- Chapters 5, 6 reports the results and key observations are discussed.
- Chapter 7 shows different ways this work can be improved while chapter 8 gives a conclusion of this thesis by summarizing the results.

2

Liver fibrosis and state of the art

In this chapter Section 2.1 gives a detailed explanation on the fibrosis disease, its causes and effects on the liver. Section 2.2 explains about the current widely used applied medical diagnosis methods to detect fibrosis, their workings along with their advantages and drawbacks. In Section 2.3 current state of the art methods in research are explained.

2.1 Liver Fibrosis

Liver fibrosis is the growth of scar tissue due to chronic inflammation [6]. Chronic inflammation can be caused due to variety of reasons like fatty liver disease, obesity, alcohol abuse, hepatitis viral infections or it can even be genetic. The scar tissue grows by replacing healthy liver cells and reducing blood flow through the liver. As a result normal functioning of the liver is affected. Progression in liver fibrosis eventually leads to cirrhosis. This is the last stage of the disease and the liver tissue is permanently scarred and it cannot be healed. Although cirrhosis can be treated with medication, treatment of advanced cirrhosis may require liver transplant. Hence determining the levels of fibrosis can indicate the severity of cirrhosis.

Figure 2.1 and shows various stages of fibrosis and Table 2.1 shows their severity. According to [6, 7], the impact of scar tissue on the liver cause the tissue to become hard with the progression of the disease. While previously it was thought that the scarring of liver is progressive and causes permanent damage to tissue, modern research [8, 9] and treatment methods show that mild to moderate levels of fibrosis recovery is possible.

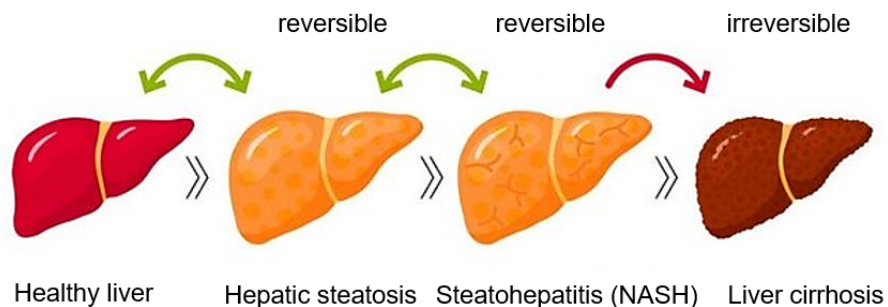


Figure 2.1: Stages of fibrosis. Source:[10]

Fibrosis stage	Severity
F0	No fibrosis
F1	Initial scarring (Mild fibrosis)
F2	Scarring extended over significant liver area (Moderate fibrosis)
F3	Different fibrotic liver areas connect by forming bridges (Severe fibrosis)
F4	Permanent liver damage with (Cirrhosis)

Table 2.1: Stages of fibrosis

2.2 Diagnostic methods of liver fibrosis

Liver Biopsy (LB): LB is an invasive medical modality that has been reliable for a very long time to detect fibrosis. See Figure 2.2. LB is also used to validate the new non-invasive modalities. In this modality, a small sample of the liver is taken by passing a needle through the abdomen. The sample is investigated using a microscope to determine the presence of inflammation and fibrotic tissues. However, this procedure suffers from drawbacks. In LB, only a small sample, 1/50000 part of liver is examined and the diagnosed result does not represent the status of whole liver due to uneven presence of fibrotic tissue and healthy liver cells [11]. A study was conducted by [12] on sampling errors during liver biopsy. The study concluded that out of 124 chronic hepatitis infected patients, 14.5% (18) of the total patients were under diagnosed of cirrhosis due to sampling error. Another serious disadvantage of this modality is its invasive nature. Liver biopsies cannot be repeated often to monitor the progression of the dis-

ease as they carry pain and bleeding complications and also involve the risk of hospitalization after the procedure due to infection. Another study conducted by [13] on complications after liver biopsy reported that 13 patients out of 405 who underwent liver biopsy were hospitalized due to these complications and reported bleeding as the most serious complication of all. The above mentioned complications indicate the need for non-invasive modalities to assess liver fibrosis.



Figure 2.2: Liver biopsy modality. Source:[14]

Blood Sampling (BS): In this modality a sample of the blood is examined to check the presence of markers that indicate fibrosis using serum biomarker algorithms [15]. See Figure 2.3. This modality is cheaper and does not involve complications as compared to a liver biopsy but it is not accurate. Parkes et al. conducted a study on the performance of serum markers [16] and concluded that only 35% of the patients could be correctly diagnosed for the presence of fibrosis but it cannot be used to identify the fibrosis stage reliably.

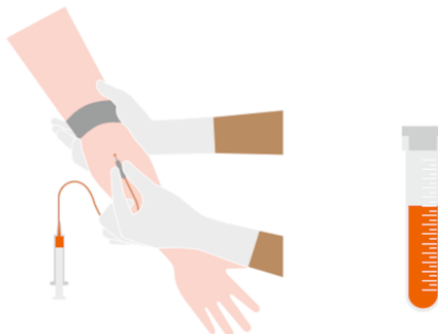


Figure 2.3: Blood sampling. Source:[14]

Ultrasound Elastography (UE): UE is an imaging technique that uses Vibration Controlled Transient Elastography (VCTE) to measure the stiffness of the liver. VCTE works by producing mechanical shear waves travel through the liver tissue and their speed is measured by the probe [17] to measure the liver stiffness. The mechanical property that shear waves travel faster in stiffer liver is used to distinguish between fibrosis stages [18]. The commonly used units for shear wave and liver stiffness is meters per second (m/s) and kilo Pascals (kPa) respectively. Fibrosis stage is determined according to the standard elasticity range of liver stiffness as shown in Figure 2.4.

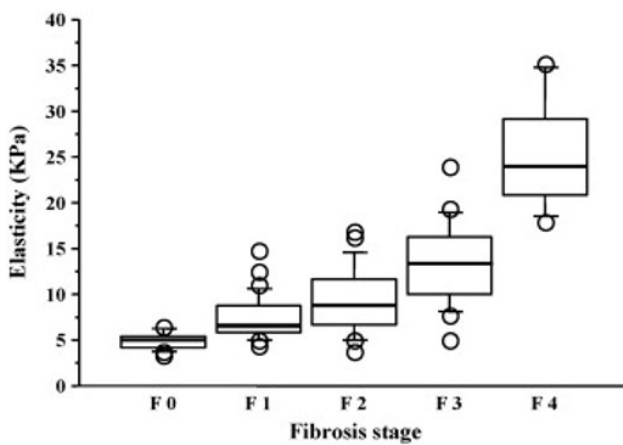


Figure 2.4: Range of liver stiffness. Source: [19]

FibroScan®[20] (refer Figure 2.5) is the name of a device that is used as gold standard for detecting fibrosis using ultrasound. As it is non-invasive and the examination volume of a FibroScan is 3.0cm^3 of liver tissue which approximately 100 times the size of a typical needle liver biopsy [21], this reduces the sampling error discussed earlier.

However, the accuracy of Fibroscan is impacted by other factors like Body Mass Index (BMI) [24] and the ongoing alcohol intake of the patient. The results are also significantly affected by the food intake hence patients are advised to avoid eating for atleast 2 to 3 hours prior to the test [25].

Magnetic Resonance Elastography (MRE): MRE is a technique that uses Magnetic Resonance Imaging (MRI) and low-frequency vibrations for non invasive mapping of tissue elasticity (see Figure 2.6). Studies have shown



Figure 2.5: FibroScan (a) and its probe (b). Sources: [22, 23]

that MRE outperforms UE in diagnosing fibrosis accurately in patients with nonalcoholic fatty liver disease [26]. It can provide three dimensional visual information about the elastic properties of the liver via elastogram that help in better diagnosis. Patients with higher BMI can also be diagnosed with better accuracy [27]. Unlike liver biopsies, MRE can be used for monitoring the disease progression [28, 29] as it can be performed multiple times

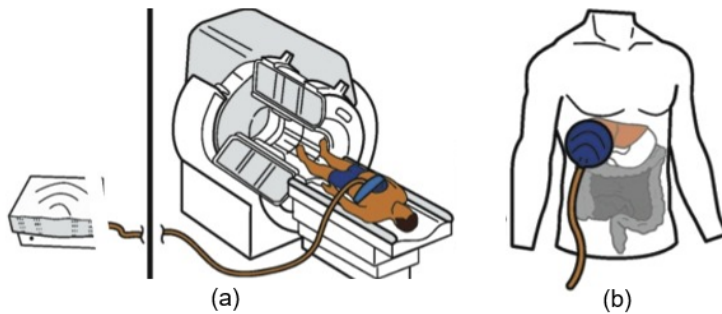


Figure 2.6: MR Elastography (a) and its probe (b). Source:[30]

As MRI technique involves powerful magnets, patients with metal or any electronic devices in body like pacemaker, cochlear implants or metallic joints cannot receive MRE test due to safety hazards. The results of patients with high levels of body iron are also difficult to interpret for the doctors because of the increased noise.

The current diagnostic methods are widely used but have their own limitations. Apart from these methods, researchers have been working on new technologies and innovating to improve the accuracy and overcome the

existing limitations. Some of the state of the art research advancements on liver fibrosis are discussed below.

2.3 State of the art in Research

FibroScan (Echosens, Paris, France) which is now a standard in non invasive methods for diagnosing liver fibrosis is based on A-mode transient elastography. FibroScan has proven to show promising results. A meta-analysis of 50 studies including a total of more than 8000 patients was conducted by Friedrich-Rust et al. [31] to assess the performance of diagnostic methods in transient elastography. It is reported that the performance of transient elastography methods are excellent and the results have high correlation with the fibrosis disease. However, FibroScan also has certain limitations like Body Mass Index (BMI) [24] as discussed earlier. Apart from these limitations, FibroScan has another serious limitation because it uses A-mode transient elastography for diagnosis. The A-mode transient elastography does not provide visual aid in locating the liver which might lead to inaccurate results as blood vessels and other tissues might be included during the assessment of liver region.

To overcome this, many research studies [32–34] are making use of B-Mode transient elastography methods that provide real-time visual aid of the region of interest while measuring elasticity to improve the accuracy. One such research work where a new transient elastography system that uses real-time B-mode ultrasound imaging for guidance was developed by Mak et al. [35]. In this work, an ultrasound transducer was specifically custom designed to work with B-mode and elastogram while measuring liver elasticity. Figure 2.7 shows the newly developed transient elastography system that provides visual guidance (Figure 2.8) to place the transducer accurately. To test the performance of LiverScan in measuring tissue stiffness, it was first tested on agar-gelatin phantoms with different stiffness and the test results were validated using mechanical indentation test. To further test the performance, in vivo assessment of LiverScan was also performed by recruiting 28 subjects for the test and the results were compared with that of FibroScan. The placement of the probe during the in vivo assessment of this study (Figure 2.9) was guided by the visual guidance interface of the B-mode transient elastography system.

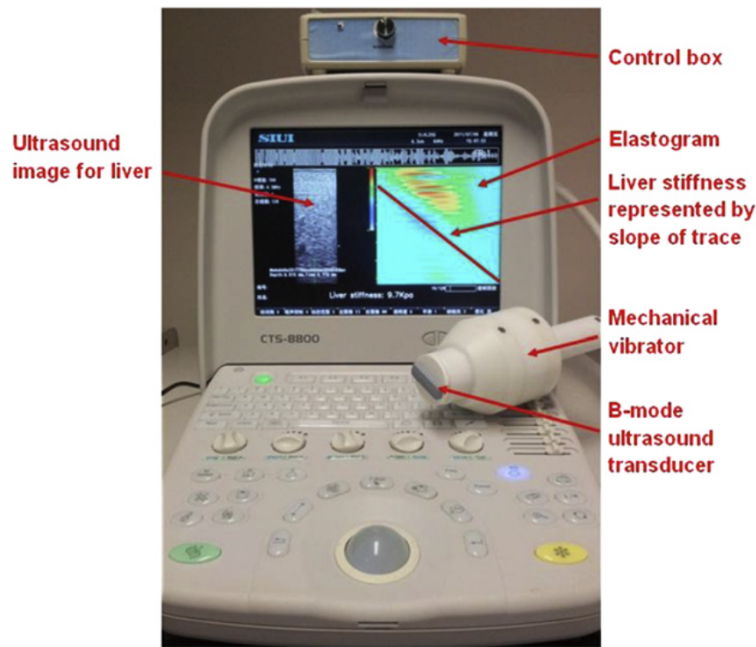


Figure 2.7: LiverScan developed by Mak et al. Source: [35]

The test results showed that values from LiverScan were significantly correlated with mechanical indentation and also with the results of FibroScan. Some values of FibroScan were higher than the values obtained from LiverScan. Further analysis has reported that the higher values from FibroScan were obtained as the probe was partially placed on diaphragm and blood vessels. This again highlights the limitation of FibroScan in lack of visual guidance for measuring liver elasticity. The results of LiverScan showed a few abnormalities where LiverScan detected high stiffness values (14.9 ± 0.7 kPa) while FibroScan reported only 5.4 kPa. To validate this inconsistency, a blood test was performed and the subject was found to be healthy. However, the reason for inconsistency was not reported. Another limitation of this study was found to be the high BMI of subjects. The visual guidance elastogram of subjects with high BMI was distorted and did not aid properly in the guidance of probe placement. While LiverScan has shown that B-mode of transient elastography can aid in visual guidance but then again the setup required for this newly developed transient elastography system is complex and requires advanced equipment. It also requires special probes of various sizes depending on the BMI of the subject while the

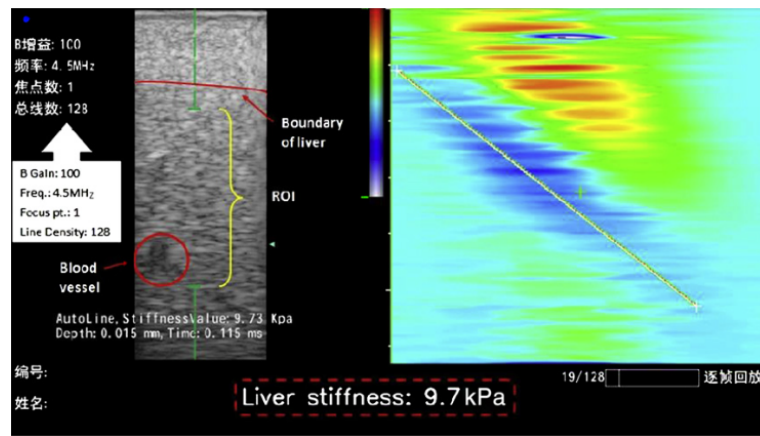


Figure 2.8: Visual guidance interface of LiverScan. Left B-mode, Right elastogram
Source: [35]



Figure 2.9: In vivo assessment. Source: [35]

visual guidance in subjects with high BMI was also distorted. These limitations are similar to that of FibroScan and do not add much contribution to the existing technology except for newly added visual guidance.

In addition to B-mode transient elastography, researchers have also been working on doppler ultrasound elastography[36–39] to improve the assessment of liver fibrosis. Regular ultrasound uses high frequency waves to produce images but they do not provide any information about the blood flow. Doppler ultrasound is a non-invasive test that gives information about the blood flow in the vessels. In case of liver, the blood flows inside

the liver through portal veins and comes out of the liver via hepatic veins. Research [40, 41] has shown that when fibrosis of liver worsens, there are significant changes in hepatic blood flow due to liver stiffness. Doppler ultrasound takes advantage of these changes that happen in hepatic blood flow to indirectly measure elasticity. Figure 2.10 shows the measurement of blood flow of right hepatic vein in liver taken using Doppler ultrasound.



Figure 2.10: Measurement of HVRI using Doppler ultrasound. Source: [37]

An observational study was performed by [37] where doppler and transient elastography (FibroScan) results of 125 patients were compared. The resistive index (HVRI) of hepatic right vein was measured and compared with the results of FibroScan. The results of this study are shown in Figure 2.11. The results show that there is a correlation between the fibrosis and the doppler measurements. Patients without fibrosis received the highest score and there is a significant difference in values of F1 and F2 fibrosis stage. Using Doppler measurements, the diameter of the portal veins was also determined and it was found that for F4 fibrotic patients, the diameter was significantly larger when compared to other stages (F0-F3) and there was a significant drop in the velocity of blood flow. Using HVRI, doppler ultrasound can be used to detect fibrosis stages of F2 and higher with high sensitivity. Although the above results show that Doppler ultrasound is a

promising way for non-invasive assessment of liver, there are many limitations to this study. Firstly, it is very difficult to find the correct vein for taking doppler measurements hence different operators might lead to different measurements. Furthermore, the authors have reported that the results are greatly influenced by the respiration rate and cardiac influx of the patients which might lead to false positives and false negatives.

Apart from these limitations, in a strong contrast, the study conducted by [42] does not agree with the results of Doppler ultrasound for estimating fibrosis. Bernatik et al. conducted a study on 43 patients using Doppler ultrasound and compared the results with liver biopsy. Unlike [37], the results of this study report that there were no significant changes in hepatic veins and the resistive indices of livers remain unaffected by fibrosis. The report also states that the doppler measurements are not suitable to estimate the degree of liver fibrosis. Hence the use of Doppler ultrasound for non-invasive assessment of liver remains inconclusive and more research is needed to draw a decisive conclusion.

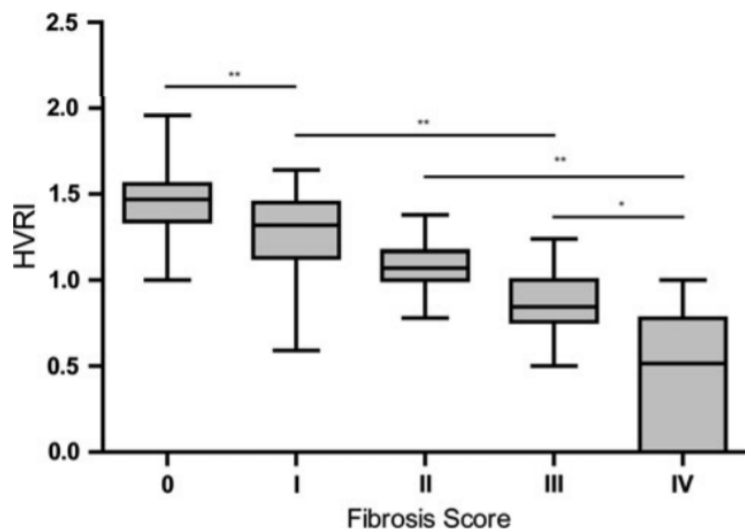


Figure 2.11: Correlation of HVRI measurements with stages of Fibrosis Source: [37]

While the above mentioned technologies deploy new and advanced hardware to measure liver stiffness, there are other research works that focus on improving the software side of the diagnostic method. With the in-

creasing popularity in machine learning and neural networks, researchers have been trying various ways to leverage this technology to tackle the challenges in medical research. He et al. [43] developed a Support Vector Machine (SVM) [44] learning model. Demographic, medical history and non-elastographic T2 weighted MRI features of 227 patients to classify the mean liver stiffness in two classes (≤ 3 and ≥ 3 kPa). To solve class imbalance problem, data balancing algorithm [45] is used for augmenting minority class (≥ 3 kPa).

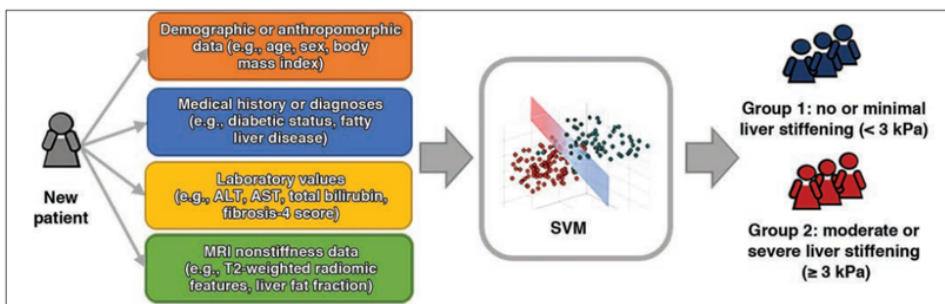


Figure 2.12: SVM model proposed in [43]

Figure 2.12 shows the schematic of the proposed SVM model. The diagnostic performance was assessed using Receiver Operating Characteristic (ROC) and Area under the ROC Curve(AUC) values and according to the results, radiomic combined with clinical features produced the best result. The combined features had an AUC of 0.84 while clinical and radiomic features independently had AUC 0.77 and 0.70 respectively.

Similar study was conducted by Hashem et al. [46] on various machine learning algorithms by combining serum biomarkers and clinical features. Genetic algorithm, alternating decision tree, multi-linear regression model and particle swarm optimization algorithms were implemented for classification of liver fibrosis (F0-F2) and (F3-F4). The dataset consisted of clinical information, laboratory tests and histological features of 39000 patients. Decision Tree algorithm performed best with 73% sensitivity. A different approach is taken by Schawkat et al. [47] by using texture based analysis derived from T1, T2 weighted MRI images for developing machine learning models to categorize the fibrosis into low-stage (F0-F2) and high-stage fibrosis (F3-F4). The study concluded that parameters derived using texture analysis from T1-weighted images can be used for identifying the

low-stage or high-stage fibrosis and that the results are comparable to MRE.

Much research [48–50] has been done on using texture based features with machine learning models and algorithms but they require input data from advanced equipment which limit their use. It also makes it very challenging task compare previous research with this work where instead of using external devices for excitation, heartbeat is used as internal excitation and regular ultrasound is used as visual input.

3

Background

In this chapter the background knowledge of essential technical concepts are explained. These concepts are fundamental to understanding the work of this thesis. An ultrasound scan of liver does not contain only liver. It consists of other body tissues and organs like heart. In order to analyze the movement of liver, the region of liver must be identified first. This is achieved using supervised deep learning. After identifying the region of liver, the behaviour of liver's movement induced by heart's excitation is analyzed using Optical Flow. This chapter is structured as follows:

In section 3.1 the technical concepts for identifying liver region are explained. Firstly, Deep Learning (DL) and the three typical learning algorithms are explained. Then we dive deeper into Image Segmentation task and eventually discuss about the architecture and components of segmentation model that is used in this work to identify liver. And finally the parameters and metrics to evaluate the model are discussed.

Section 3.2 explains how Optical Flow (OF) is used to track the movement of objects in a sequence of images. Further, OF is executed on a test video not only to visualize its working but also to understand the output generated by OF.

3.1 Deep Learning

Artificial Intelligence (AI), *Machine Learning* (ML) and *Deep Learning* (DL) are most common and yet most confused terms in this area of research due to nuances between them. AI is a broad discipline of science that studies different ways to build programs that become smarter with experience. ML is a technique to realize AI by training algorithms to make better deci-

sions. DL is a subset of ML that is inspired by the working of human neural system and its neurons. DL makes use of Artificial Neural Networks (ANN) that can filter and classify high level features from data by passing it between neural layers. Figure 3.1 describes this relation between AI, ML and DL.



Figure 3.1: Relationship between AI, ML, NN and DL. Source:[51]

3.1.1 Types of Learning

As discussed in section 3.1, ML requires data to learn the patterns hidden in the data. Based on how the model learns these patterns, the learning techniques can be classified in four different ways: *Supervised Learning* (SL), *Semi-Supervised* (SSL), *Unsupervised Learning* (UL) and *Reinforced Learning* (RL). In SL, the data provided to the model consists of input data along with its corresponding output. While training the model, it learns a mapping function that maps input to output. SL can further be grouped into Classification and Regression. In UL, the data provided to the model consists only of input, i.e. the data is unlabeled. In this case the model learns the structure or distribution of data. UL can further be grouped into Association Learning, Anomaly Detection and Clustering. See figure 3.2 In SSL, the data provided to the model consists of both labeled and unlabeled data. This type of learning is used when labeled data

is hard to gather. Hence these models make use of partially labelled data to improve the model's performance. SSL models are used in speech analysis, General Adversarial Networks (GANS), and internet content classification. In RL, the model learns through a series of rewards and penalties. These rewards and penalties are called as reinforcements. Some of the RL algorithms are State-Action-Reward-State-Action (SARSA) and Q-Learning.



Figure 3.2: Examples for supervised and unsupervised learning. Source:[52]

3.1.2 Image Segmentation

In the image classification task, each input image is assigned to a class. However, image classification is not sufficient to determine where the object is located in the image. This can be achieved using Image Segmentation (IS) by assigning a class label to each pixel of the image. IS can be used to identify the location of an object, its shape and also to identify the class of each pixel of the input image. IS is achieved by training the model to generate segmented masks where each pixel of the mask is assigned to a label. The input, label and expected output of an IS model can be easily understood from figure 3.3

Some of the state-of-the-art models for image segmentation are, Fully Convolutional Network (FCN) by [53], U-Net by [54] and Feature Pyramid Network (FPN) by [55]. U-Net model was specifically designed to work on medical images using very few annotated samples. This is similar to the

nature and size of the dataset of this work. Hence U-Net model is used for this work. Section 3.1.4 explains the U-Net model, it's architecture, working, layers and other components in detail.



Figure 3.3: Input, label and output of segmentation model. Source:[56]

3.1.3 Metrics for Image Segmentation

The performance of an IS model can be quantitatively measured by performing certain pixel wise operations. The most common metrics used in IS are Pixel Accuracy, Jaccard Index and Dice Coefficient.

- Pixel Accuracy: It simply evaluates to the percent of pixels that are correctly classified. For binary mask, this can be calculated as

$$\text{accuracy} = \frac{TP + TN}{TP + TN + FP + FN} \quad (3.1)$$

- Jaccard Index: It is also known as Intersection-over-Union (IoU). This evaluates to the percent overlap between the predicted and target mask.

$$IoU = \frac{|target \cap prediction|}{|target| \cup |prediction|} \quad (3.2)$$

- Dice Coefficient: It is also known as F1 Score and is very similar to Jaccard Index. It measures the overlap of prediction and ground truth.

$$Dice = \frac{2 * |target \cap prediction|}{|target| \cup |prediction|} \quad (3.3)$$

3.1.4 U-Net for Image Segmentation

As discussed in section 3.1.2, the U-Net model by Ronneberger et al. [54] is an IS model with a symmetrical architecture created specifically for segmentation of bio-medical images. The left part is called *Convolution* while the right part is called *De-Convolution*. The convolution, also called as downsampling/contraction is responsible for extracting features from the image using convolution layers. This process is similar to an image classification model. The de-convolution, also called as upsampling/expansion uses transposed convolution to increase the resolution of the image while reducing feature maps and improving localization. Further more, the convolution process is connected to de-convolution via so called *Skip Connections* that prevent loss of information. This type of model architecture is called as Encoder-Decoder architecture. SegNet [57] and RefineNet [58] are other examples of Encoder-Decoder architecture. The layers and activation functions of U-Net model are explained below.

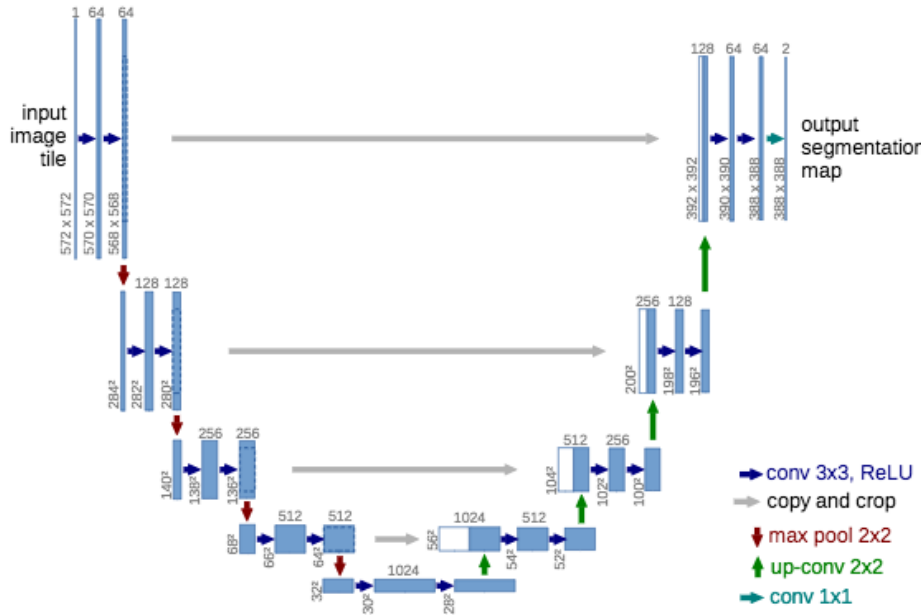


Figure 3.4: Architecture of Unet Model. Source: [54]

3.1.5 Layers

- **Convolution Layer:** For a 2D image, a Convolution operation slides a filter over the input data with a series of pixel wise operations that result in a single output. The filter is called as *Kernel* and the size of kernel defines the field of view of the Convolution. The number of pixels the filter must slide along a dimension after calculating the kernel output is called *Stride*. During this process when the kernel is at the border of input, *Padding* appends data along the border to the input to perform the Convolution. The output of all kernel operations combine to result in a matrix with different set of features and reduced spatial dimensions. Hence this operation is also called as Downsampling.
- **Transposed Convolution Layer:** The output of Image Segmentation model is usually a segmented mask with the same size as the input image. However, while extracting features using Convolution, the size of the matrix reduced. In order to restore its spatial dimensions while maintaining the extracted features, Transposed Convolution is performed. The working and parameters of Transposed Convolution is same as as Convolution. Figure 3.5 visualizes Convolution and Transposed Convolution.
- **Pooling Layer:** Pooling layers are generally used to summarize presence of features in a feature map. Average and Max pooling are the most widely used methods. U-Net model uses max pooling with a pooling size of 2x2. Refer figure 3.6

3.1.6 Activation Functions

An Activation Function (AF) defines what a neuron/node should output depending on the weighted input that the neuron receives. AF summarizes the weighted input and gives a single output. Generally non-linear AF are used in neural networks as they can model complex patterns hidden in data. Some of the most common activation functions are explained below.

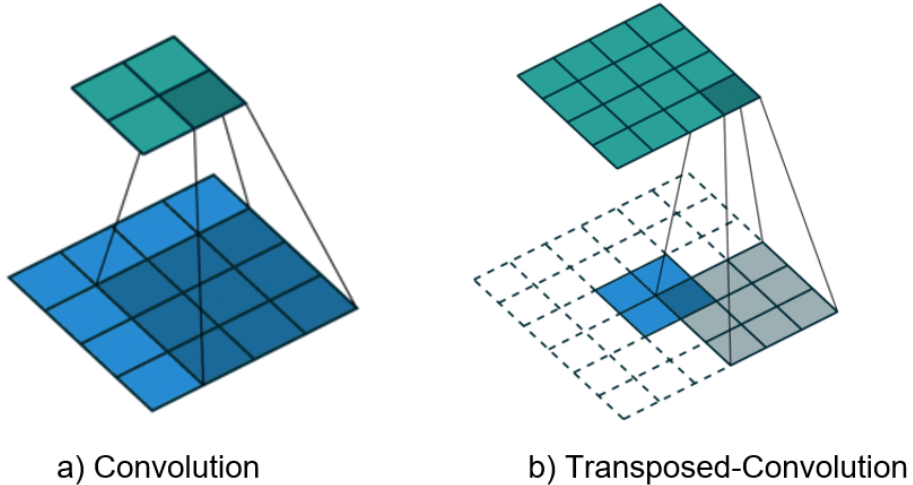


Figure 3.5: Convolution and Transposed Convolution with a 3X3 kernel and a stride of 1

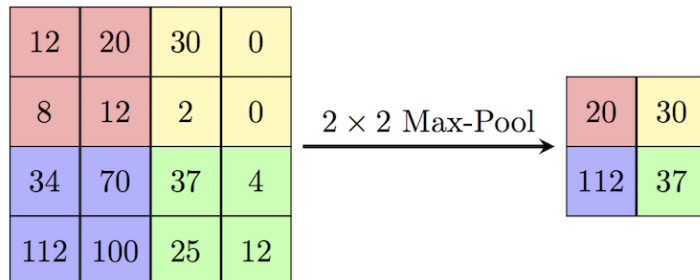


Figure 3.6: Max Pool with 2x2 pool size. Source:[59]

- **Sigmoid:** It is non-linear and generally used when the expected output is a probability. i.e., the output of Sigmoid lies between 0 and 1. It is also called as Logistic Activation Function.

$$\text{Sigmoid : } S(x) = \frac{1}{1 + e^{-x}} \quad (3.4)$$

- **ReLU:** Rectified Linear Unit (ReLU) AF behaves as a linear AF in the positive axis but overall it is non-linear AF bounded between 0 and infinity. ReLU AF converges faster than sigmoid function and results in sparse activations of the neural network. Hence this is widely used

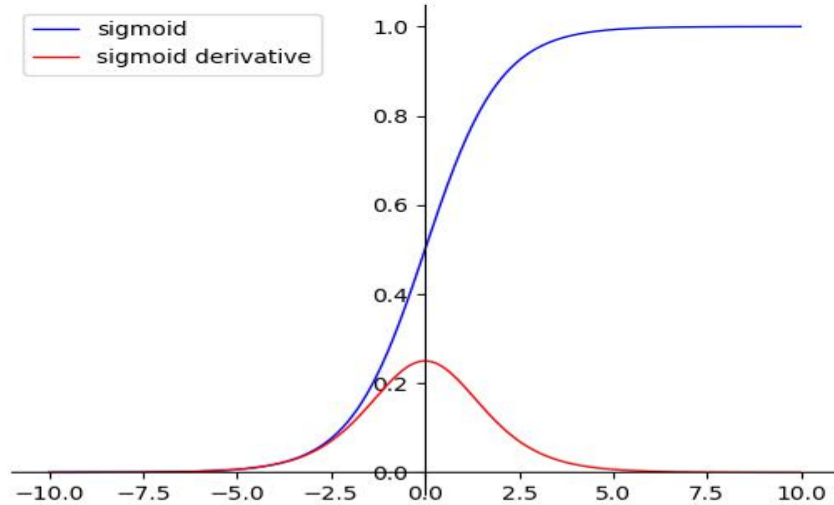


Figure 3.7: Sigmoid Activation Function. Source:[60]

in Deep Neural Networks. However, for negative inputs, the gradient becomes zero. This means that the weights of neuron in this region never get updated and do not respond to variations in input. Thus the neuron becomes "dead" and never learns. This is called as *Dying ReLU* problem. This can be solved with a subtle change from ReLU's equation 3.5 to equation 3.6 by introducing a constant gradient alpha. This is called as Leaky-ReLU.

$$\text{ReLU} : R(x) = \max(0, x) \quad (3.5)$$

$$\text{Leaky-ReLU} : R(x) = \max(\alpha x, x) \quad (3.6)$$

- **ELU:** Exponential Linear Unit (ELU) by [61] is similar ReLU. It solves the problem of vanishing gradients by introducing non-zero gradients at all negative values. The computation time of ELU is slower than other AF but it converges faster while training.

$$\text{ELU} : E(x) = \begin{cases} x & \text{if } x \geq 0 \\ \alpha e^x - 1 & \text{if } x < 0 \end{cases}$$

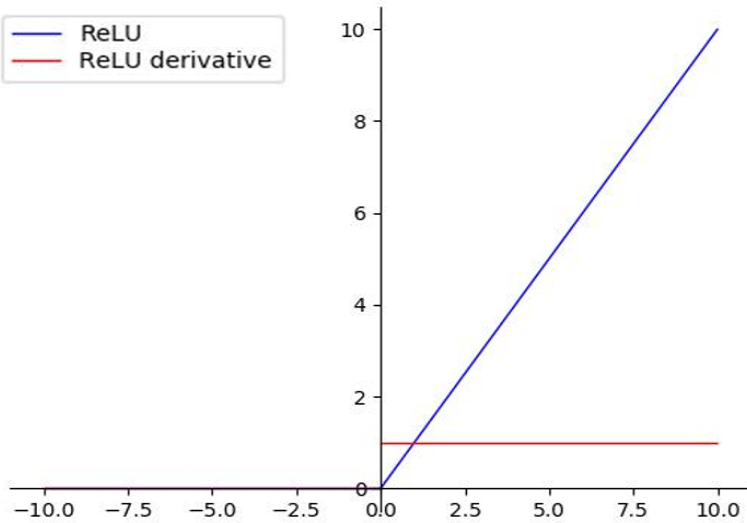


Figure 3.8: ReLU Activation Function. Source:[60]

3.1.7 Loss Functions

Neural Networks use stochastic gradient descent to optimize the learning process. Neural network uses the current set of weights and calculates the error. The gradient of the error is calculated and updates the weights accordingly to reduce the error in next evaluation. The function that calculates this error is called Loss Functions (LF).

- **Cross-Entropy:** This is a loss function that is generally used in classification models whose output is a probability of that instance belonging to that class. The equation for calculating average loss is given by 3.7

$$Loss = -\frac{1}{N} \sum_{i=1}^N \sum_{j=1}^k t_{i,j} \log(p_{i,j}) \quad (3.7)$$

Where:

- N is the number of samples
- k is the number of classes
- $t_{i,j} = 1$ if instance i is in class j and 0 otherwise
- $p_{i,j}$ predicted probability that sample i belongs to class j

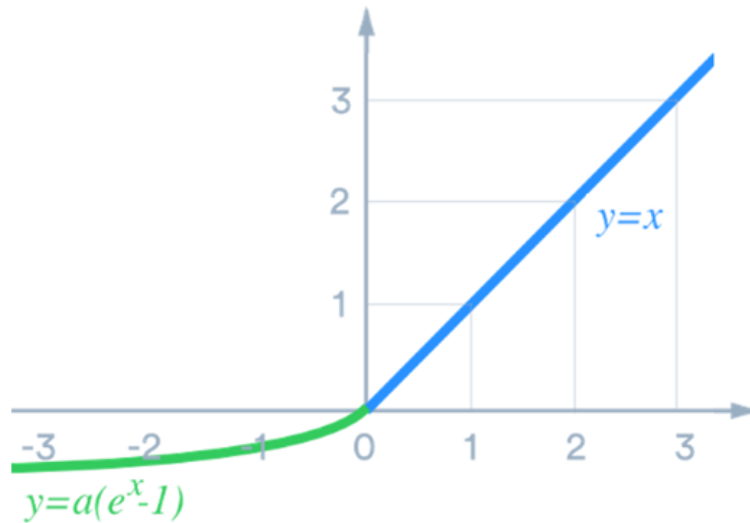


Figure 3.9: ELU Activation Function with alpha=1. Source:[62]

Cross entropy is a loss function used for balanced datasets. However when the classes are imbalanced, the neural network gets stuck at a local minima and classifies all the pixels of the image to the major class. Tversky loss overcomes this issue.

- **Tversky loss:** Tversky loss is the complement of Tversky Index(TI). TI is very similar to Dice Coefficient (eqn 3.3). Two parameters α and β are added to the equation. Depending on the use case, these parameters can be changed to penalize False Positives or False Negatives.

$$\text{Tversky Index} = \frac{TP}{TP + \alpha FN + \beta FP} \quad (3.8)$$

Where $\alpha + \beta = 1$

If $\alpha > \beta$ then False Negatives receive higher penalty than False Positives. Tverky loss is given by:

$$\text{Tversky Loss} = (1 - TI) \quad (3.9)$$

3.2 Optical Flow

Optical Flow (OF), also known as Motion Detection, is one of the key topics in the field of Computer Vision. The aim of OF is to detect and track the position of a moving object or features of an object in a sequence of images. The applications of range from vehicle control [63] to detecting objects in front of a vehicle [64], from tracking human skeleton [65] to tracking face [66].

There are two main types of OF algorithms. Sparse and sense. A sparse OF calculates the flow vectors only for the pre-defined set of pixels. These pre-defined set of pixels can either be specified explicitly or obtained from another algorithm like Harry corner [67] detection algorithm. Dense OF calculates flow vectors for all the pixels of the image. Although Dense OF is slow during computation it is known to have higher accuracy than Sparse OF.

The main assumption of these algorithms is that the intensity of an object remains same. i.e., the pixel intensities are constant between the frames. The working of OF can be explained clearly from figure 3.10.

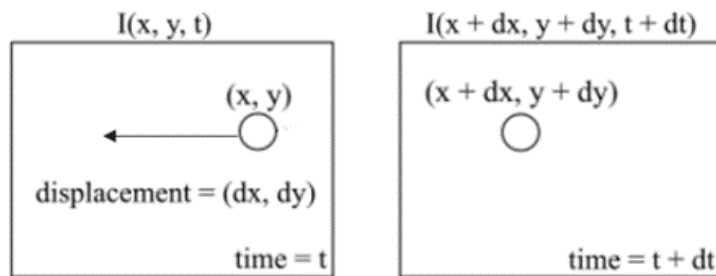


Figure 3.10: Optical Flow Problem

The intensity of an object's pixel I can be expressed with three parameters x, y, t where x, y are coordinates of pixel at time t . The intensity of the object after a displacement of dx, dy over time dt is $I(x+dx, y+dy, t+dt)$. Equation 3.10 summarizes this.

$$I(x, y, t) = I(x + dx, y + dy, t + dt) \quad (3.10)$$

3.2.1 Optical Flow with an example

In this section, the Farneback algorithm which is a dense optical flow method from OpenCV [68] which is an open source python library is tested on a video to have a better understanding. In the video sequence the car travels from right to left (Figure 3.11a). A mesh grid is created for visualizing the flow maps (Figure 3.11b). Each point of the grid represents a flow vector of that pixel that gives information on its angle and magnitude of movement. On close observation, the flow vectors with non-zero magnitudes are represented by arrows where the size represents magnitude and direction of the arrow represents angle of movement.

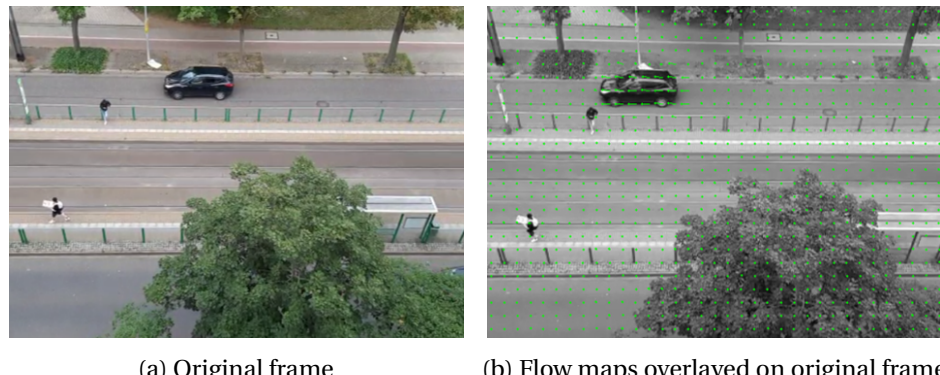


Figure 3.11: Testing Optical Flow for a moving car

OpenCV library supports the following parameters for creating flow maps of an image sequence.

- **levels:** Image pyramids are created by stacking layers of the images to estimate the translation of feature points. The size of the pyramid is given in this parameter.
- **pyr_scale:** This parameter gives the scale of next level in the pyramid.
- **winsize:** It is the size of the window for searching the feature in next frame.
- **iterations:** The number of iterations to be performed at each level

- **poly_n:** OF uses polynomial expansion between pixels to track features. This parameter is the size of pixel neighborhood used in polynomial expansion.
- **poly_sigma:** It is the standard deviation of Gaussian while calculating the polynomial expansion.

4

Materials and Methods

This chapter gives an overview of the procedures executed to test the hypothesis of this work i.e, a soft healthy liver would absorb the heart's excitation better than a hard fibrotic liver. As the distance from heart's region of excitation increases, there is a decrease in excitation. Hence from the hypothesis, the decrease in heart's excitation on a healthy liver would be more than that of a fibrotic liver. Figure 4.1 gives a brief overview of the procedures to prove this hypothesis. Each procedure, its input and output data is detailed in the following sections. First, a segmentation model is trained to identify the region of liver in a set of images of an ultrasound video and optical flow is used to create flow vectors of the entire ultrasound video. Flow vectors contain data about the angle and magnitude of movement of the entire ultrasound scan including liver. Using the segmentation video, initial observers are placed at the region of heart's excitation. Once the initial observers are placed, flow vectors are used to find the angle of movement for each initial observer. A trajectory is projected along the angle of movement for each initial observer. Then non-initial observers are placed along each trajectory across the entire liver. After placing the initial and non-initial observers, flow vectors of all the observers are extracted and processed for further analysis. The structure of this chapter is described below.

In this chapter, section 4.1 describes the acquisition of data and medical diagnosis procedure followed to determine the fibrosis stage of liver. Pre-processing of dataset and training a segmentation model is explained in section 4.2. Section 4.3 describes how the liver's movement is tracked using OF to determine it's angle and intensity of movement by placing trajectories of *Observers* in the direction of liver's movement starting from the

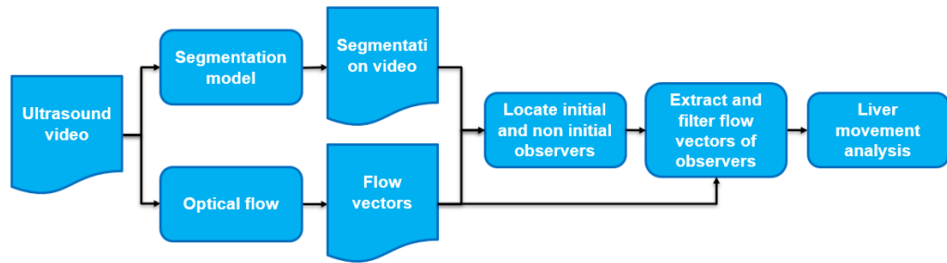


Figure 4.1: Block diagram of the method

region of excitation. Section 4.4 explains the expected results that were arrived based on hypothesis and evaluation of above methods.

4.1 Data Acquisition

The dataset consists of diagnostic details of the livers of 15 unique patients. Dataset Table 4.1 consists of liver stiffness, it's fibrosis stage. Liver stiffness is measured in kilo Pascal (kPa) using FibroScan®(Echosens, Paris, France) [20]. The fibrosis stage is determined by an expert doctor in this field according to the standard cut-off values (Table 4.2) of fibrosis and medical history of the patient. Their ultrasound videos of liver including heart was also acquired at 30fps (frames per second). The final column is the number of ultrasound videos of that patient. Table 4.2 shows the standard ranges of liver stiffness for each fibrosis stage depending on the disease of the patient. The range of liver stiffness for a normal person is between 3.9 -5.3 kPa [69].

The study was performed according to the World Medical Association Declaration of Helsinki - Ethical Principles for Medical Research Involving Human Subjects. All subjects included in the study provided written informed consent and the study protocol was approved by the local Institutional Review Board of Otto-von-Guericke University of Magdeburg.

4.2 Liver Segmentation

This section explains the procedures for training a segmentation model to identify the region of interest i.e. liver, using deep learning. The pur-

Patient_ID	Liver stiffness	Fibrosis stage	# of samples
Pid_002	4.0 +/- 0.7	F0/F1	2
Pid_004	6.7 +/- 3.7	F2	2
Pid_005	69.2 +/- 31.0	F4	3
Pid_007	2.8 +/- 0.6	F0/F1	2
Pid_008	9.5 +/- 0.9	F2	3
Pid_009	27.4 +/- 11.4	F4	3
Pid_010	6.6	F0/F1	3
Pid_011	65.2 +/- 8.2	F4	3
Pid_012	3.9 +/- 0.7	F0/F1	2
Pid_013	5.2 +/- 1.4	F0/F1	2
Pid_014	8.5 +/- 1.7	F2	2
Pid_015	12.0 +/- 1.3	F3	2
Pid_016	5.0 +/- 1.5 (SW)	F0/F1	3
Pid_017	50.2 +/- 30.3 (SW)	F4	3
Pid_018	5.3 +/- 2.5 (SW)	F0/F1	2

Table 4.1: Liver stiffness and fibrosis stages dataset

Liver disease	Fibrosis stage			
	F0 to F1	F2	F3	F4
Hepatitis B				
Hepatitis C	2 to 8	8 to 10	10 to 14	14 or higher
HIV (co-infection)				
Cholestatic liver	2 to 7	7 to 9	9 to 17	17 or higher
NASH or NAFLD	2 to 7	7 to 10	10 to 14	14 or higher
Alcoholic Hepatitis	2 to 7	7 to 11	11 to 19	19 or higher

Table 4.2: Standard cutoff values. Source: [70]

pose of a segmentation model is to aid in placing initial and non initial observers inside the liver. Section 4.2.1 explains the preparation of dataset while section 4.2.2 explains about network architecture, its metrics and the predictions of the trained model.

4.2.1 Preparing the dataset

A supervised image segmentation model requires images and their masks for it's training. This section explains how the 37 ultrasound scans are pre-processed from videos to images and labels to feed the model. Figure 4.2 shows this process.

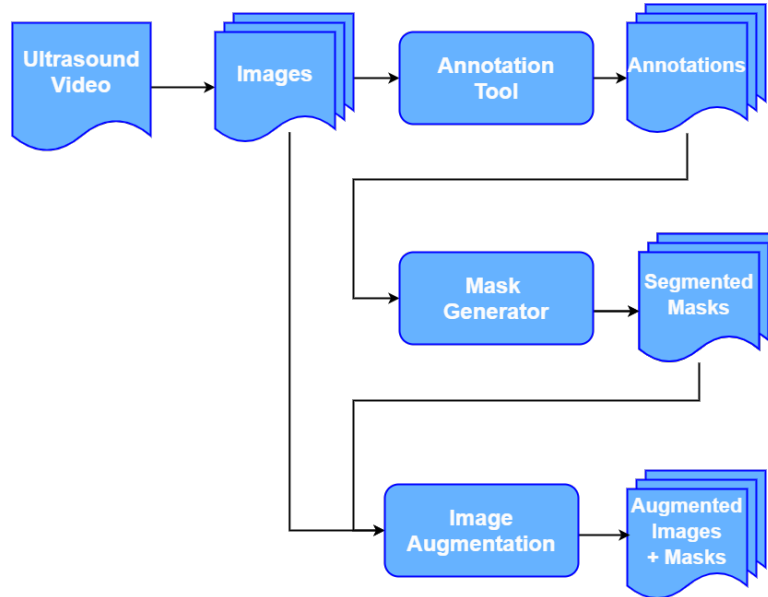


Figure 4.2: Dataset preparation

From each of 37 ultrasound scans a snapshot of the scan is taken at every 30th frame, i.e. every one second. These frames are then used to create annotations using the VASA annotation tool [71]. Figure 4.3 shows the VASA annotation tool along with the annotations for Pid_010.

The annotation tool outputs the pixel coordinates of the annotation in the form of a comma-separated-values (.csv) file. These annotations are then used to create binary segmentation masks of the liver which serve as ground truth to the model.



Figure 4.3: VASA annotation tool

A total of 300 annotations are created using the annotation tool. As only a coarse estimate of liver boundary was needed for creating the dataset of segmentation model, the boundaries were marked by the author of this thesis and not by medical expert. Ultrasound videos were used as reference while marking the annotations. The model was initially trained on this data for 20 epochs but it resulted in low validation accuracy (60%). Hence the size of the dataset is increased using basic data augmentation techniques like dropout, sharpening, rotation and contrast enhancement. In summary, 300 original and 900 augmented images, i.e. 1200 images are used for training the model.

4.2.2 Training segmentation model

As the size of the dataset is small and model is binary, a U-Net model with base 4 and batch size 16 is created using Keras [72] and Tensorflow [73] python libraries. 60% of data is used for training the model while remaining is used for validation. Table 4.3 shows other hyperparameters that are required to set the network. Weight initialization plays an important role in training a model. Hence weights are initialized using He normal distribution proposed by He et al. [74] to speed up the training process. It takes variance of the dataset into account and initializes the weights accordingly.

Hyperparameter	Setting	Hyperparameter	Setting
Activation function	ELU	Dropout rate	0.1
Weight initialization	He normal	Optimizer	Adam
Padding	Same	Initial learning rate	1e-4
Stride	2	Final activation function	Sigmoid
Kernel size	(3 x 3)	Loss function	Tversky loss

Table 4.3: Hyperparameters for segmentation model

Figure 4.4 shows the learning curve of the segmentation model. Dice coefficient is used as accuracy measure to evaluate the model's performance. Initially dice coefficient was also used as loss function while training but this resulted in a model getting stuck at local minima as there is class imbalance in the dataset. To elucidate this local minima, the model would classify all the pixels in the image as non-liver and achieve 70% accuracy right from the first training epoch.

To overcome this, Tverksy loss [75] with $\alpha = 0.3$ is used. This means that the model is penalised more if pixels belonging to liver are not classified correctly. The model is trained for 20 epochs but an early stopping mechanism is used where the model stops training if the accuracy of validation set does not improve much. The best model achieved an accuracy of 92% and loss of 5%.

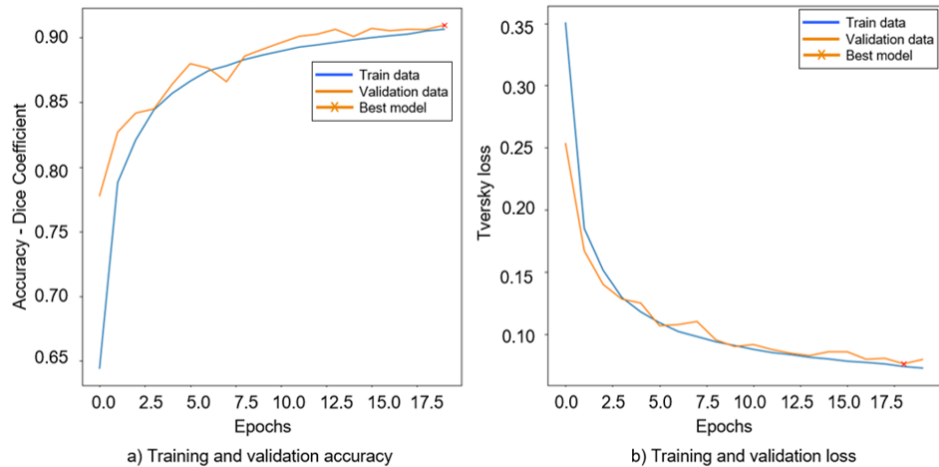


Figure 4.4: Learning curve of segmentation model

The model's predictions on validation set after training are visualized in Figure 4.5. The input given to the model is labeled as X and the model's prediction is labeled as y -predicted.

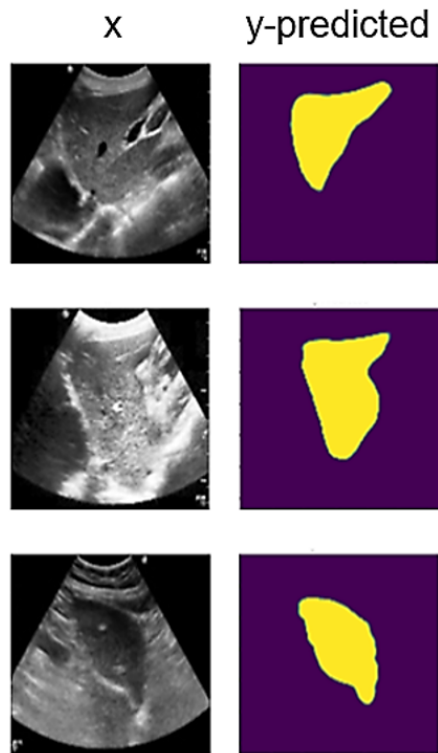


Figure 4.5: Model predictions

4.3 Liver Movement Assessment

4.3.1 Location of Initial Observers

The direction of liver's movement can be assessed by placing multiple so called *Initial Observers* within a single image. An observer is a window that captures the movement of a specific region over the set of images of one scan as flow vectors. The flow vectors contain information about the direction and magnitude of movement of each pixel where the observer is placed. The initial Observers are placed along the border of the liver where the heart comes in contact with liver during the cardiac cycles. This

region is called as region of excitation. It is also observed that this region has more movement when compared to other sections of the liver.

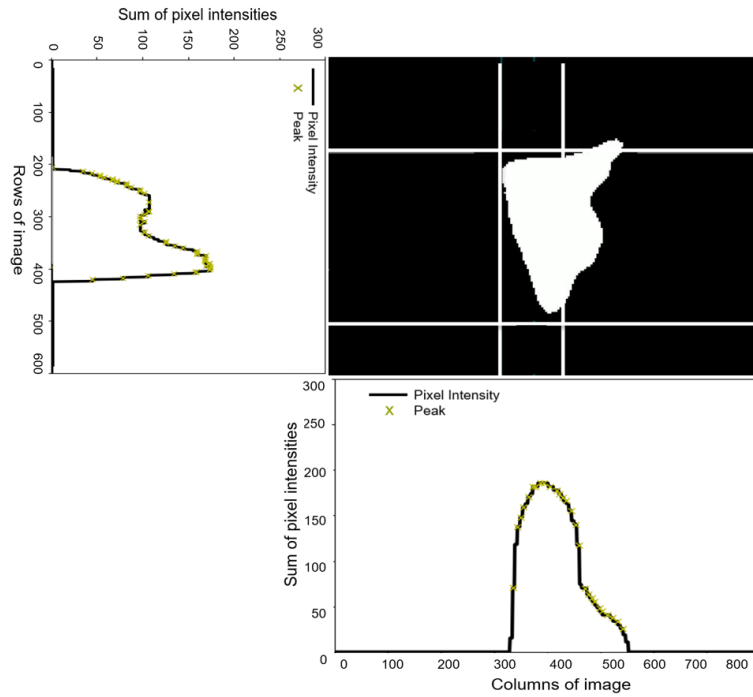


Figure 4.6: Region of excitation detection

To find the region of excitation, row and column wise sum of pixel intensities is performed and peak detection algorithm from SciPy [76] python library is executed. This can be visualized from Figure 4.6. The first and last peak of the row wise sum of intensities are extracted. The location of these peaks indicate the beginning and end of the liver as one scans the image from top to bottom. However, for the column wise sum of intensities, only the first peak is extracted. A buffer of ≈ 100 pixels is added to this and the intersection of these four locations results in a bounding box of the region of excitation. The size of buffer is not fixed and varies for each ultrasound scan depending on the shape of the liver.

After finding the region of excitation edge detection algorithm by [77] is used to find the edges of liver. This gives pixel coordinates of the liver's boundary. A simple logical AND operation of the bounding box calculated previously and the liver's boundary gives the boundary of the region of excitation.

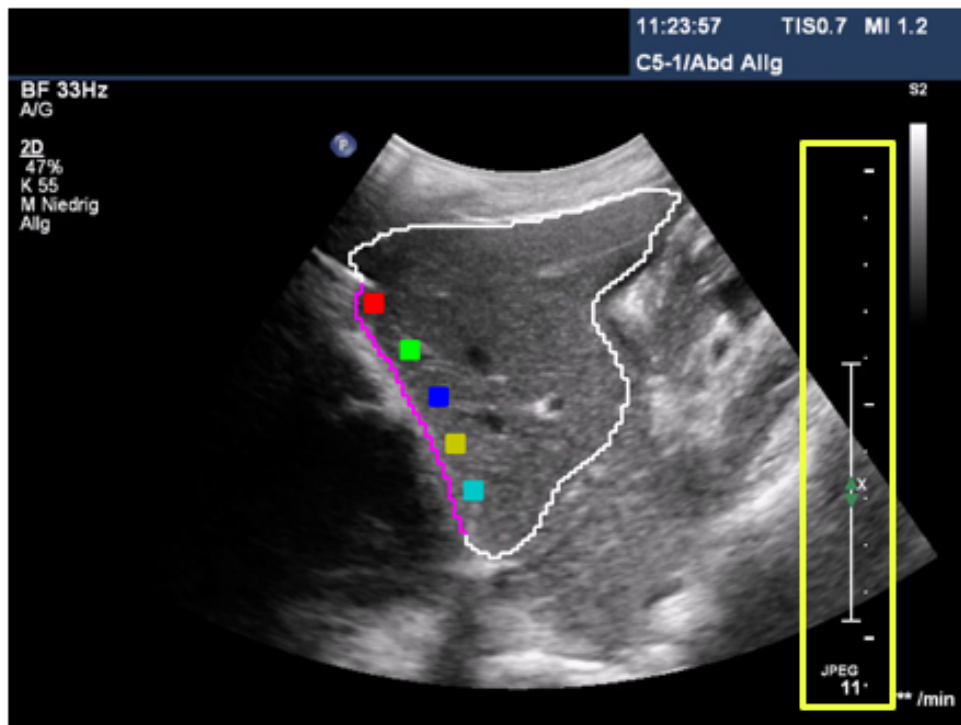


Figure 4.7: Location of initial observers

Figure 4.7 shows the location of initial observers along the liver's boundary. The ultrasound scans usually have a scale (highlighted in yellow in Figure 4.7) that indicate the physical dimensions during the diagnosis of this liver. The number 11 indicates that the scale is of 11 centimeters in total. Using this scale, the number of pixels per centimeter can be found. By counting the number of pixels between the *dashes* in the scale it is observed that ≈ 39 pixels is one centimeter. The conversion factor varies for each ultrasound scan and the pixels per centimeter conversion factor ranges roughly from 32-42 pixels for a scale range of 10-14. This conversion factor is important as it allows the observers to be placed at equal distances even if the ultrasound scans are recorded at a different scale. The observers are placed at a distance of 1 centimeter from each other across all the ultrasound scans during this work.

Parameter	Value	Parameter	Value
levels	3	iterations	3
pyr_scale	0.5	poly_n	5
winsize	15	poly_sigma	1.2

Table 4.4: Parameters of optical flow API of OpenCV library [68]

4.3.2 Estimation of Liver's Movement Trajectory

The magnitude and angle of movement of each observer is recorded using optical flow. Table 4.4 shows the parameters used for calculating the optical flows using the OpenCV library [68]. These parameters are explained in section 3.2.1 and the values were obtained on experimental basis. The angle of movement of all the initial observers of an ultrasound scan can be visualized in Figure 4.8. The x-axis of this image represents the angle of movement. The angles range from 0 to 360 degrees and y-axis represents the frames an ultrasound scan. This plot shows the angle of movement for five observers across 220 frames. However this data is filled with noise. The noise is visible as sudden rapid spikes in the angle of movement. The understanding and reasoning behind this noise is that the heart's excitation displaces the liver and when heart contracts, the liver returns to its original position. When liver is at its extreme position after excitation, the angle of movement is stable. As the heart contracts, the liver starts to return to its original position. As liver starts to reach its original position, the angle of movement begins to spike. When the liver starts to displace again with the next excitation, the spike drops and the angle of movement starts to stabilize.

To make it easier to visualize, the magnitude and angle of movement of a single observer is shown in Figure 4.9. To eliminate the noise generated due to small displacements, a threshold value of 3 pixels is set on the magnitude. This means that flow vectors whose magnitudes of displacement greater than 3 pixels are used in further analysis. The average of extracted angles is used as the movement trajectory of that specific region where the observer is placed. As the boundary of liver is already known using deep learning, the approximate end of trajectory can also be known. Figure 4.10 shows the location and trajectory of each initial observer. This extraction

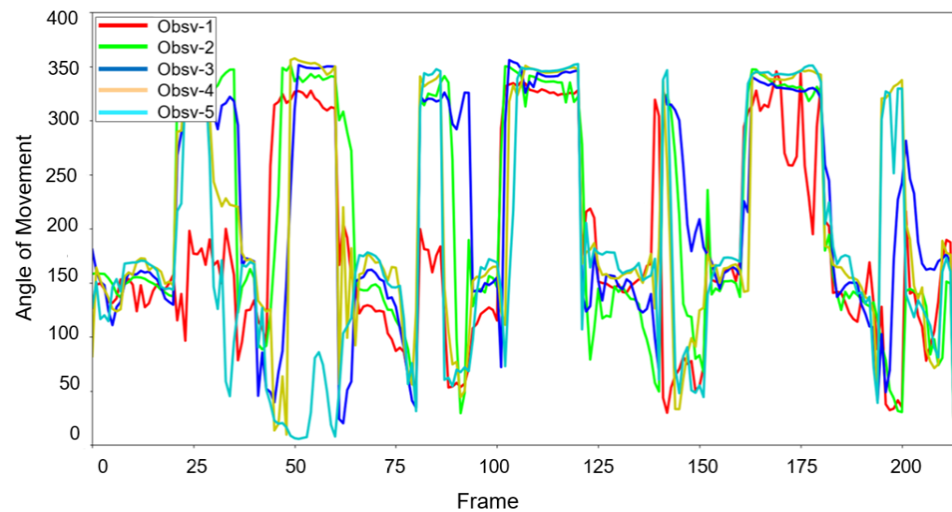


Figure 4.8: Angle of movement of initial observers

is done for all the initial observers hence each observer has it's own angle and trajectory of movement.

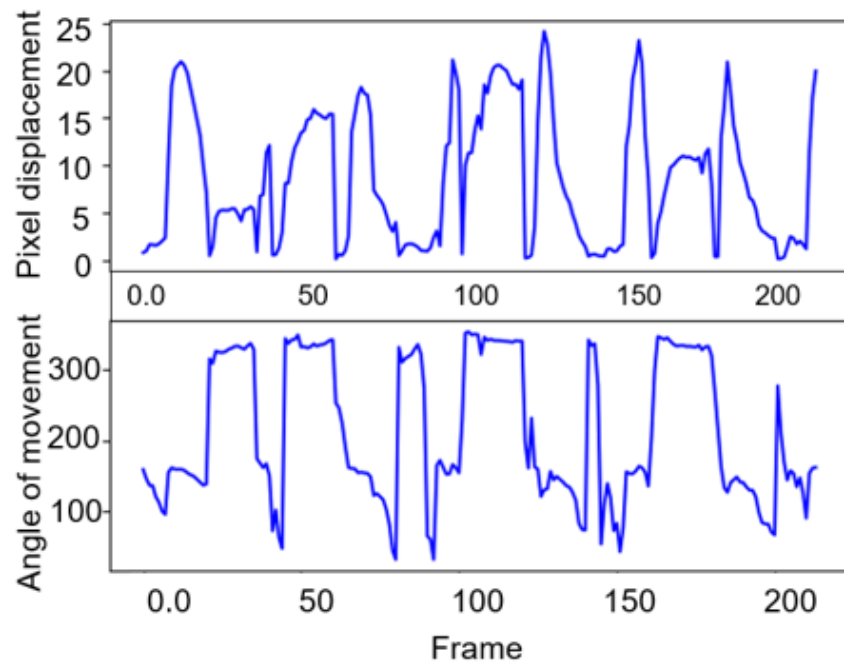


Figure 4.9: Flow map of initial observer

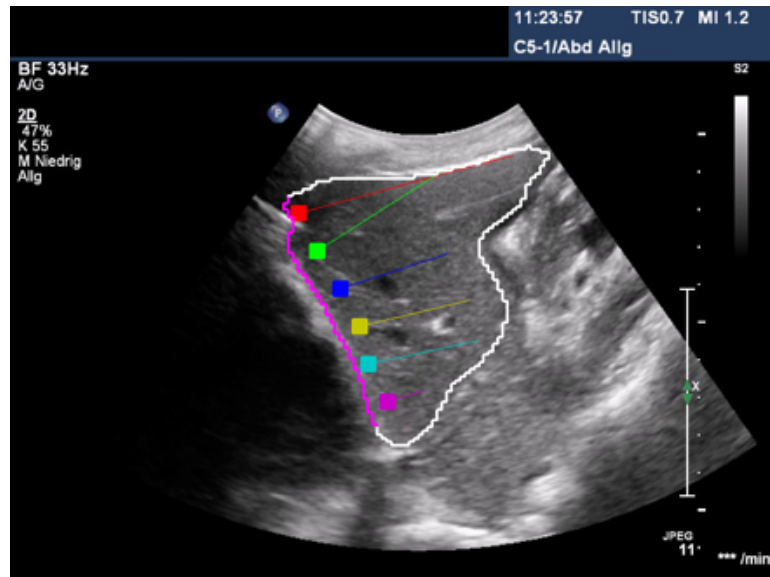


Figure 4.10: Trajectories of movements in the liver

4.3.3 Computation of Intensity

Once the trajectory of movement for each initial observer is determined, more observers are placed on each trajectory such that they span across the liver starting from the region of excitation. These new observers are referred to as *non-initial* observers and are placed along the trajectory at a distance of 1cm from each other. Figure 4.11 shows the placement of non-initial observers along the trajectory. Each observer records the average magnitude of movement of that region for all the frames. The magnitude of movement is recorded for both initial and non-initial observers. As discussed earlier, the noise is eliminated by setting the threshold value. This means that only flows greater than the threshold are used for further analysis.

4.4 Evaluation Procedure

This section is based on evaluating the methods to verify the hypothesis described in section 1.1, i.e. to discover if a healthy liver absorbs the heart's excitation better than a hard fibrotic liver. The heart excites liver through heartbeat. In the liver, as the distance from region of excitation increases

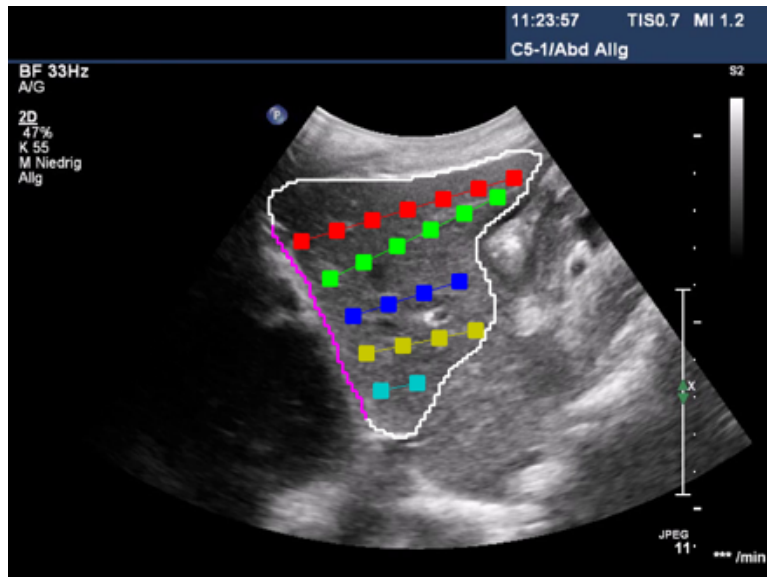


Figure 4.11: Initial and non-initial observers

there is decrease in excitation. This decrease in excitation is called damping. According to the research [78, 79] conducted on fibrotic livers, as fibrosis gets severe, the liver starts to lose its elasticity and becomes stiff. Hence a healthy liver which is soft might have high damping when compared to an unhealthy liver. The hypothesis can be visualized in Figure 4.12. The figure shows the before and after of heart's excitation in healthy liver and fibrotic liver. A healthy liver would absorb more energy from the excitation than the stiff fibrotic liver.

On the basis of hypothesis, the expected results are shown below. The Figure 4.13 represents expected results for a healthy liver (a) and an unhealthy liver (b) with three trajectories each. The x-axis represents distance from initial observer in centimeters while y-axis represents percentage decrease in magnitudes with respect to the magnitudes of initial observer. After performing liver movement analysis of all the livers individually, multi-liver correlation analysis is performed to compare all the livers across all stages of fibrosis (Figure 4.14). This is achieved by averaging the damping of all the trajectories of a liver and comparing it with other livers. The expected result is that the percentage decrease in magnitudes will be very less in fibrotic livers while healthy liver will have high percentage decrease in magnitudes indicating better absorption of heart's excitation.

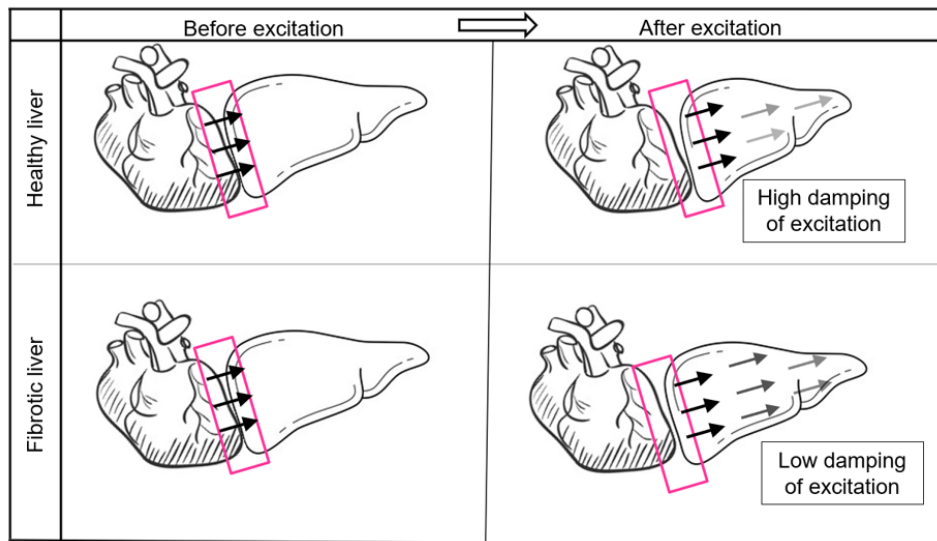


Figure 4.12: Hypothesis visualization

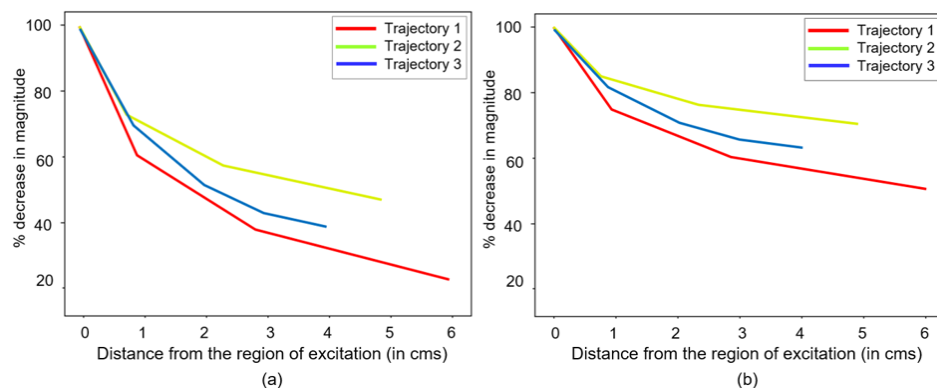


Figure 4.13: Expected damping of trajectories in healthy liver (a) vs fibrotic liver (b)

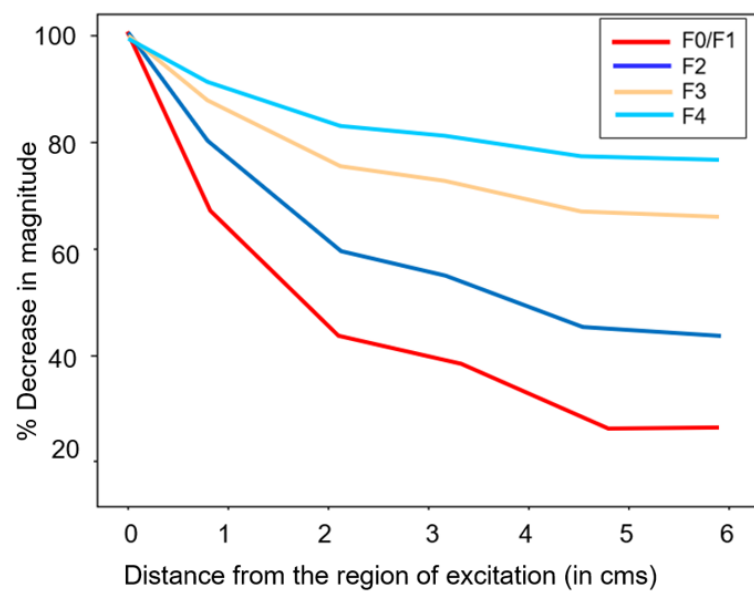


Figure 4.14: Expected damping of magnitudes at various fibrosis stages

5

Results

This chapter shows the results that were obtained after performing movement analysis of the liver. Section 5.1 initially shows the spread and distribution of the magnitudes of liver's movements using box plots. Then the damping of heart's excitation of all the livers of the dataset are also shown in individual plots in this section while section 5.2 combines the individual damping plots grouped by their fibrosis stage. And finally the results of all the livers are visualised in a single plot to give a bigger picture on the damping at all the stages of fibrosis.

The threshold constraint set earlier to eliminate the noise where magnitudes greater than the threshold value (3 pixels) are taken into consideration is shown in figure 5.1. This figure shows pixel displacement and its angle of movement for 220 frames for a single observer. The pixel displacement values which are greater than the threshold are marked as black points in the plot. It can also be seen that the sudden change in angle of movement due to smaller magnitudes of movement are also eliminated - highlighted in red after subjecting it to threshold constraint.

5.1 Liver Movement Analysis

As discussed in section 4.4, the movement of liver is tracked after placing initial and non-initial observers along the trajectory of movement. Figure 5.2 shows the box plot of magnitudes for Pid_010 which is an healthy liver. The box plot helps in understanding the distribution of magnitudes recorded at the observers. The y-axis represents the the magnitude of liver movement and the x-axis represents distance from the region of excitation. The distance is measured in centimeters (cms), hence 0 on x-axis

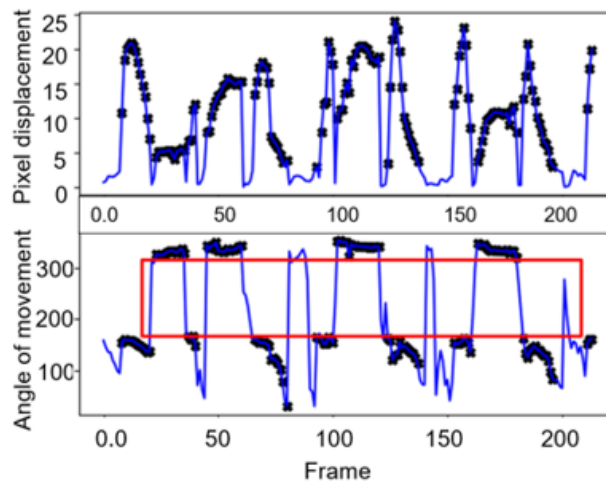


Figure 5.1: Flow map of one observer and threshold values

represents all the initial observers that were placed along the region of excitation while other non-zero values on x-axis represent non-initial observers grouped by their distance from the region of excitation. The values of this plot are the magnitudes of liver's movement that were obtained after subjecting to the threshold constraint.

The box plot shown in Figure 5.2 is of an healthy liver with F0/F1 fibrosis stage. As it is an healthy liver, there is significant decrease in the magnitudes as the distance from the region of excitation increases. This decrease in the magnitudes is referred to as damping of heart's excitation. When the same analysis is performed on an unhealthy liver with fibrosis stage F4 (Figure 5.3), the damping is very less and almost similar order of magnitudes is observed even if the distance from the region of excitation is increased. This trend of damping indicates the presence of credibility in the hypothesis that a healthy liver which is soft would absorb the heart's excitation better than a hard fibrotic liver.

To visualize the damping of heart's excitation, the decrease in the mean values of magnitude with respect to the initial observers is plotted. For all the 15 patients, this analysis was performed. The placement of observers and their resultant damping is shown in figures 5.4,5.5,5.6.

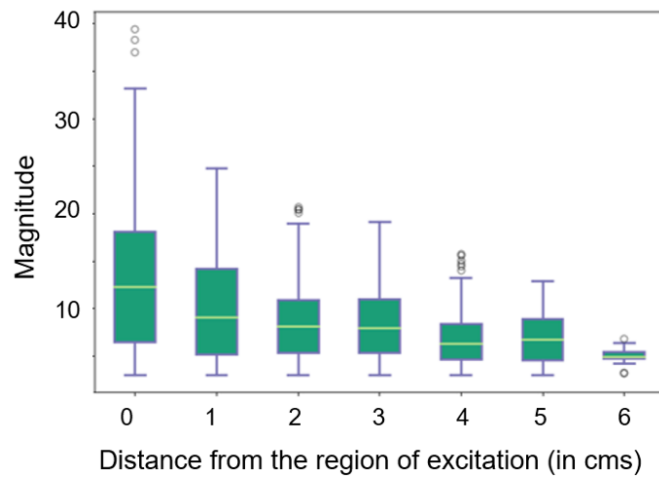


Figure 5.2: Box plot of magnitudes for healthy liver (F0/F1)

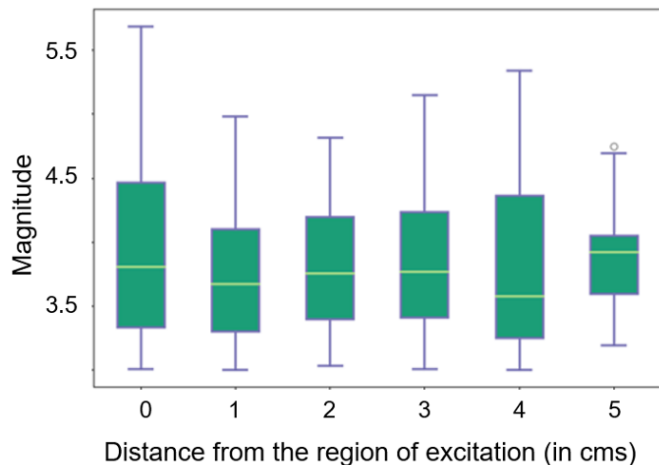


Figure 5.3: Box plot of magnitudes for fibrotic liver (F4)

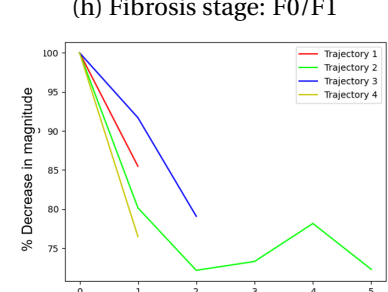
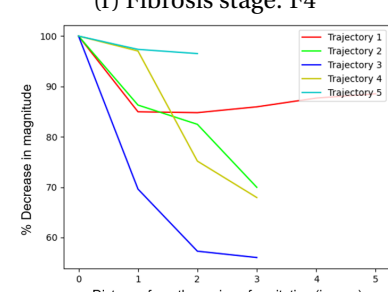
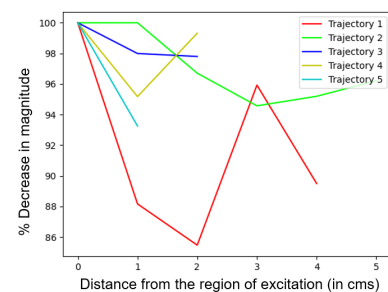
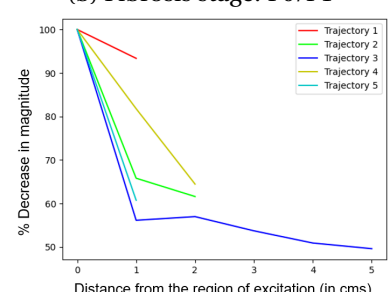
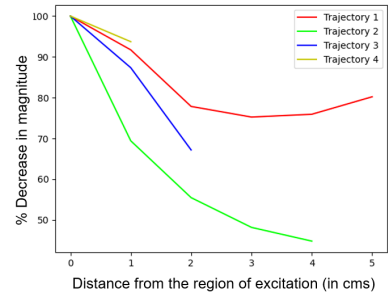
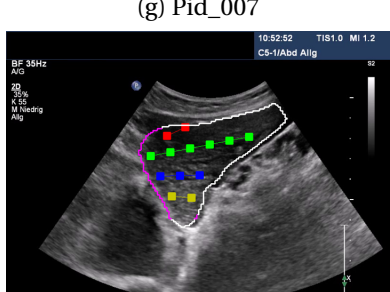
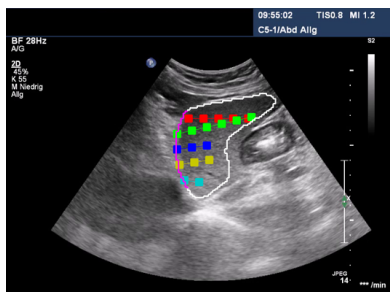
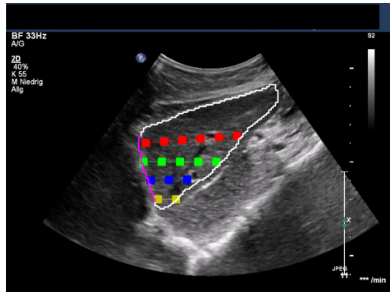


Figure 5.4: Observer placement and their damping of mean of magnitudes(1)

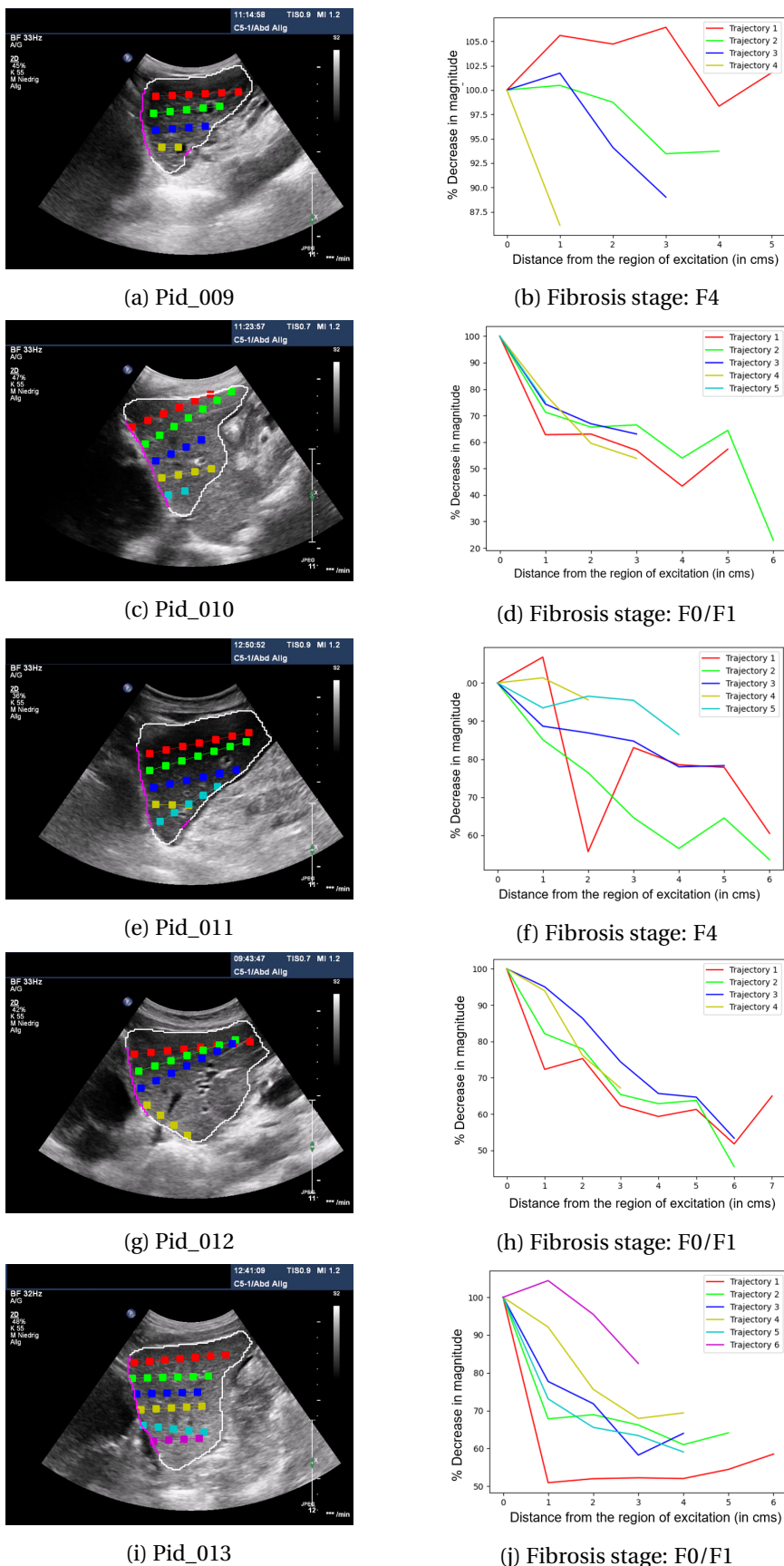
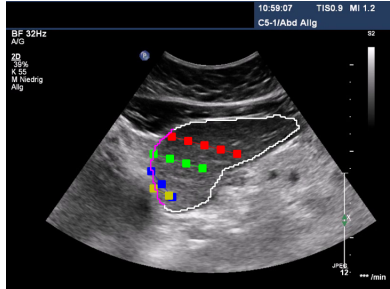
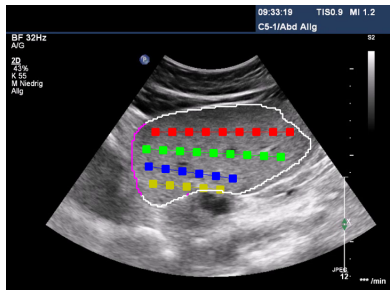


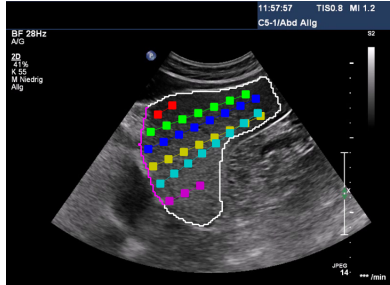
Figure 5.5: Trajectories and their damping of mean of magnitudes(2)



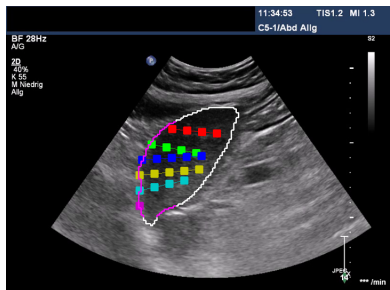
(a) Pid_014



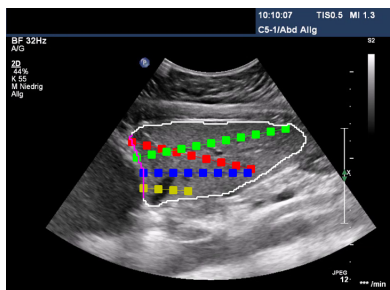
(c) Pid_015



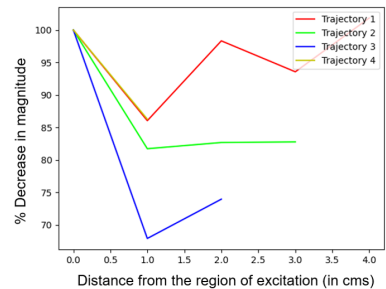
(e) Pid_016



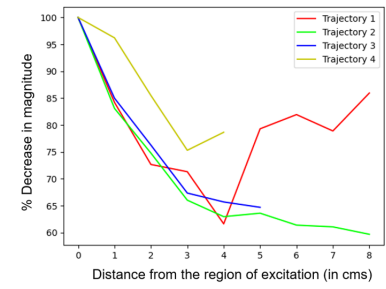
(g) Pid_017



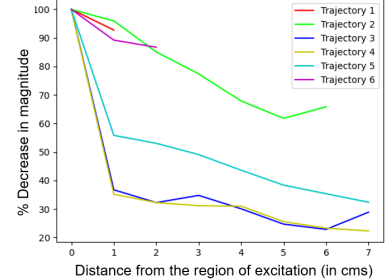
(i) Pid_018



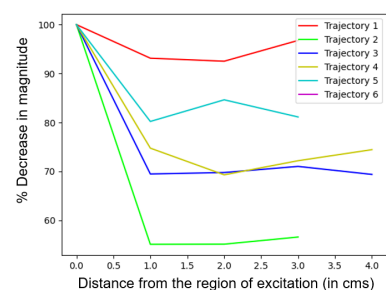
(b) Fibrosis stage: F2



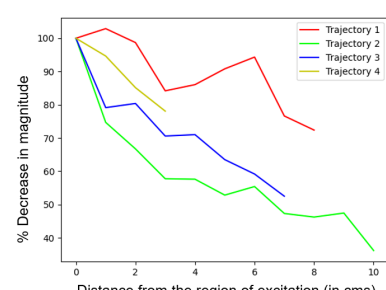
(d) Fibrosis stage: F3



(f) Fibrosis stage: F0/F1



(h) Fibrosis stage: F4



(j) Fibrosis stage: F0/F1

Figure 5.6: Observer placement and their damping of mean of magnitudes(3)

5.2 Multi-Liver Correlation Analysis

Figure 5.7 shows line plots of all the livers at all fibrosis stages. Each subplot visualizes the damping of all trajectories of the livers grouped by their fibrosis stage.

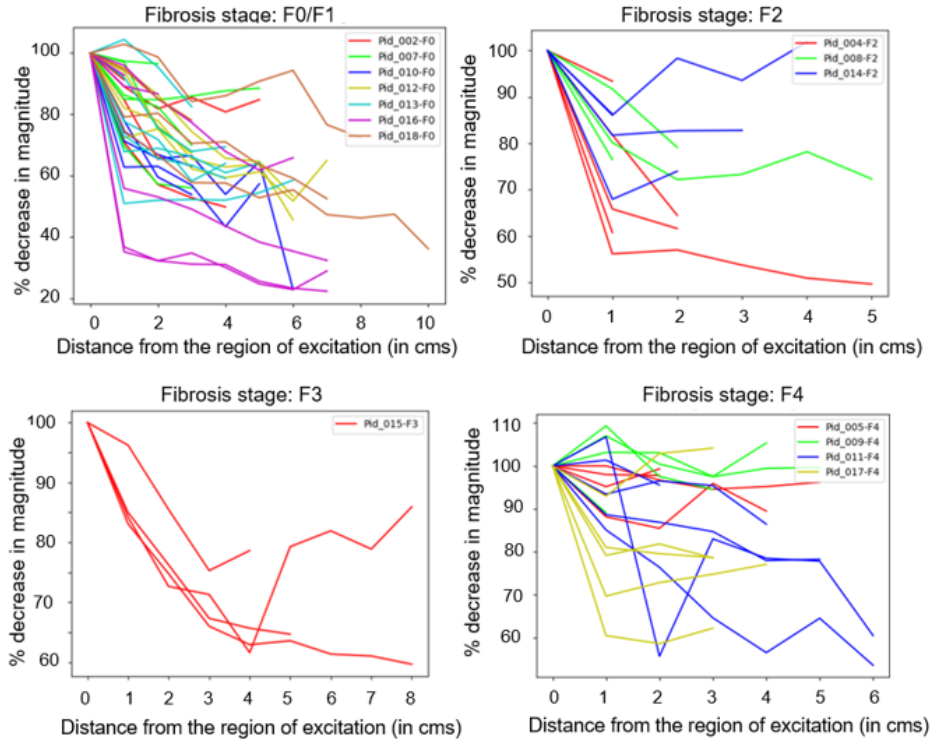


Figure 5.7: Damping of mean of magnitudes of fibrotic stages

To simplify and summarize the above four sub plots, for each fibrosis stage, the average damping of trajectories is taken. This results in each fibrosis stage having its own damping as shown in Figure 5.8. For each fibrosis stage in Figure 5.7, the damping values of each liver are shown as box plot in Figure 5.9. The average damping of mean of magnitudes from the initial observer is observed to be 69%, 80%, 77% and 88% for F0/F1, F2, F3 and F4 respectively.

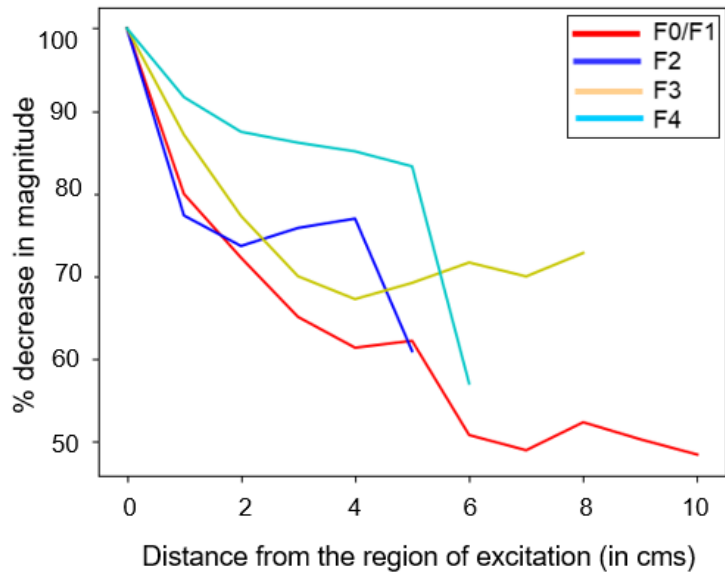


Figure 5.8: Average damping of fibrosis stages

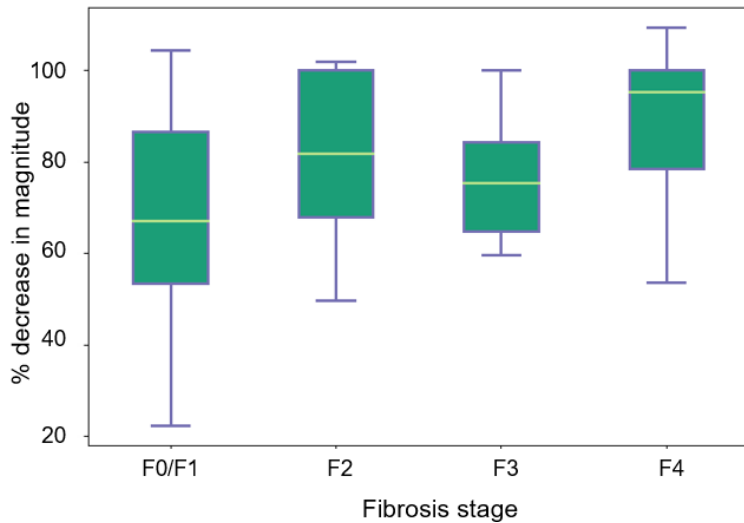


Figure 5.9: Box plot of stage wise damping values

6

Discussion

In this work, ultrasound scans of 15 patients were analyzed and their damping across the liver from the region of excitation was recorded. The damping was recorded by projecting trajectories in the direction of liver's movement. During the analysis most of the trajectories indicated that the magnitudes of liver movement decrease as the distance from the region of excitation increases. Some abnormal behavior of the trajectories is also observed. There is an increase in magnitudes for some of trajectories (Pid_005, Pid_011) after the region of excitation. The increase in magnitudes can be explained based on the working of optical flow algorithms. Optical flow methods are good in tracking objects if the intensity of the object remains same. If the line of trajectory passes through liver regions where there is high change in intensity then this behavior is observed. Apart from this, the damping of a trajectory was higher in case of Pid_009 due to unstable ultrasound scan while rest of the ultrasound scans seemed to be stable visually.

The following section focuses on answering the research questions.

Research Questions:

- **Is optical flow combined with deep learning methods suitable to relate liver's movement with its fibrosis stage?**

Yes, optical flow and deep learning methods are suitable to relate liver's movement with its fibrosis stage although there are certain limitations with regards to optical flow. Ultrasound scans render organs and tissues as points of variable brightness. However, if the region of interest is dark then optical flow is unable to measure the magnitudes properly. This is observed in Pid_011 and Pid_017. The magnitude of movement observed in these two ultrasound scans is

very low resulting in high noise. The magnitude of pixel displacement was so low that the threshold value for eliminating noise had to be reduced for these ultrasound videos. Another drawback observed here is the change in intensity in specific regions of liver that can be caused due to the presence of serrations in liver. In such cases, optical flow methods can be improved by smoothing the image and reducing the variation of intensities.

- **Is it possible to estimate liver's fibrosis stage using only ultrasound scans?**

The results have shown that there is a significant difference in damping across between various fibrosis stages except for the difference between F2 and F3. Given the current dataset, this method can potentially be used to identify low-stage (F0/F1) or high-stage (F2-F4) fibrosis but not the exact fibrosis stage. A decisive answer to this research question can be found by analyzing large dataset while maintaining class balance across all the fibrosis stages. Apart from this, the figure 5.9 shows an increasing trend in the damping of magnitudes as the fibrosis stage progresses from F0 to F4.

- **Can the use of advanced hardware be minimized in detecting liver fibrosis?**

Detection of fibrosis requires advanced technological hardware. Devices like FibroScan®[20] use controlled vibrations to generate excitations, other devices like MRE use vibrations induced by magnetic resonances and some detect fibrosis by identifying the blood flow in hepatic veins. All of these devices use an external device for inducing excitations externally one way or other. Without using any external hardware for inducing excitation in the liver, the results of this work have shown that there is a relation between the movement of liver and its fibrosis stage. This relation shows that there is a way and this relation can be strengthened with more research to detect the exact stage of fibrosis. With more research it can be proved that the special probes for excitation can be minimized however this method would still require input from the regular ultrasound device.

7

Future Work

The results of this work prove that there is a relation between fibrosis stage and it's liver movement and it can be clearly seen while comparing the results of F0 and F4 fibrosis stages. The damping decreases as the fibrosis worsens from F0 to F4 except for F3 fibrosis stage. As the size of dataset is small, the analysis could be performed only for 15 patients. The size of the dataset is not only small, it also has the problem of class imbalance. The number of ultrasound scans with F0 fibrosis is 7 while only 1 patient with F3 is available analysis. Hence more samples and well balanced dataset would definitely contribute in making the results more decisive.

The current dataset of ultrasound scans is taken at 30fps. Increasing the frame rate of ultrasound scans can improve the output of optical flow methods in estimating the magnitudes and angle of movement of the liver. Although initial and non-initial observers allow to analyze certain portion of liver but they do not cover entire liver. Figure 7.1 shows the distribution of magnitudes for Pid_017, the outliers indicate high levels of magnitude. Similar behavior is observed during the analysis of other ultrasound videos. By increasing the size of observers adjusted along the complete liver boundary as shown in figure 7.2 such that more liver tissue can be analyzed will make the results more stable. But this would require an accurate segmentation model where ground truth for segmentation model is labeled by experts from medical background.

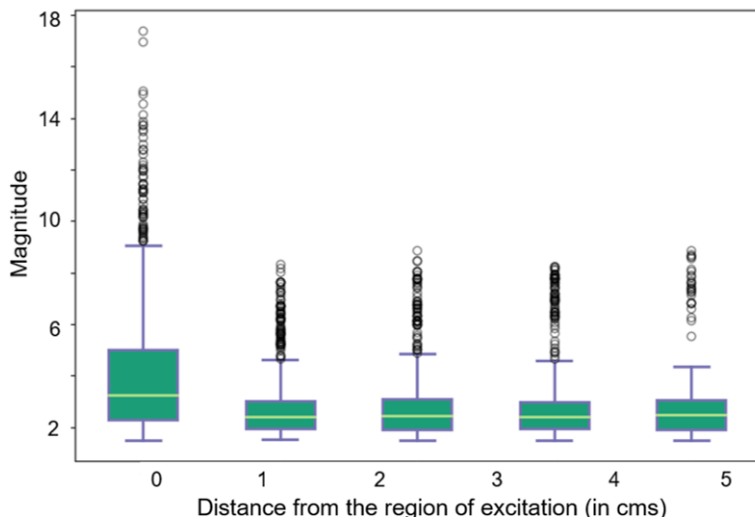


Figure 7.1: Box plot of magnitudes for Pid_017

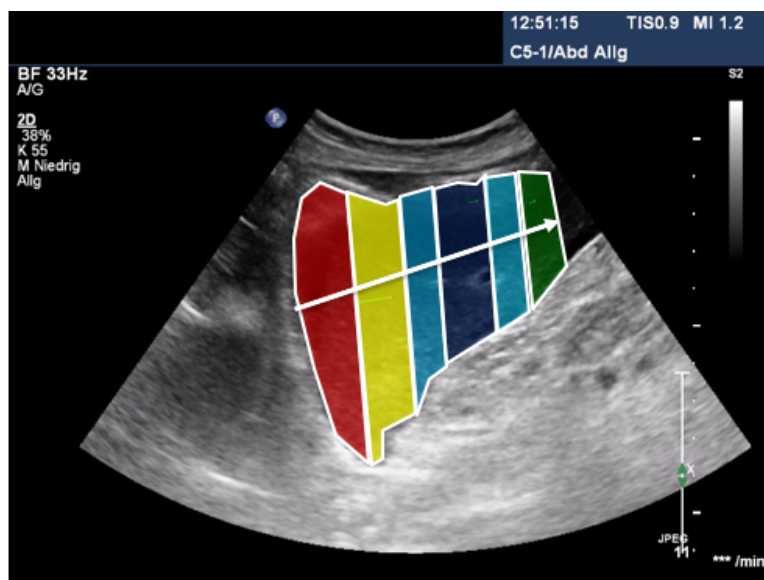


Figure 7.2: Possible observers for future analysis

8

Conclusion

In this thesis, the results prove that a relation could be established between liver's movement and it's fibrosis stage by using deep learning and optical flow methods while using heartbeat as internal excitation from the ultrasound scans. The region of interest which is liver is identified using U-Net deep learning model and liver's movement is tracked using optical flow methods to explore solutions for specific research questions. Using the current available dataset, the mean damping of fibrosis stages from the region of excitation is measured. The average damping for F0/F1, F2, F3 and F4 liver is observed to be 69%, 80%, 77% and 88% respectively. Although the difference between the results of F0/F1 stage livers and F4 stage livers is clearly distinguishable, determining the exact fibrosis stage of the liver remains a challenging task.

The result of this thesis is suitable for the current dataset and it is uncertain if it can be applied to external data due to the size of current dataset (15 patients). If more data could have been used then this experiment would have a promising developing prospects. However, the findings and conclusions of this research will be helpful to other fellow researchers to find a way in future that could potentially avoid liver biopsies, minimize the use of advanced medical equipment and perform liver analysis by using the regular ultrasound device thereby reducing the cost, effort and time in medical diagnosis.

A

Abbreviations and Notations

Acronym	Meaning
LB	Liver Biopsy
BS	Blood Sampling
UE	Ultrasound Elastography
VCTE	Vibration Controlled Transient Elastography
kPa	kilo Pascals
BMI	Body Mass Index
MRE	Magnetic Resonance Elastography
MRI	Magnetic Resonance Imaging
SVM	Support Vector Machine
ROC	Receiver Operating Characteristic
AUC	Area under the ROC Curve
AI	Artificial Intelligence
ML	Machine Learning
DL	Deep Learning
ANN	Artificial Neural Networks
SL	Supervised Learning
SSL	Semi-Supervised
UL	Unsupervised Learning
RL	Reinforced Learning
GANS	General Adversarial Networks
SARSA	State Action Reward State Action
IS	Image Segmentation
FCN	Fully Convolutional Network
FPN	Feature Pyramid Network
AF	Activation Function
ReLU	Rectified Linear Unit
ELU	Exponential Linear Unit
LF	Loss Functions
TI	Tversky Index
OF	Optical Flow

B

List of Figures

2.1 Stages of fibrosis. Source:[10]	4
2.2 Liver biopsy modality. Source:[14]	5
2.3 Blood sampling. Source:[14]	5
2.4 Range of liver stiffness. Source: [19]	6
2.5 FibroScan (a) and its probe (b). Sources: [22, 23]	7
2.6 MR Elastography (a) and its probe (b). Source:[30]	7
2.7 LiverScan developed by Mak et al. Source: [35]	9
2.8 Visual guidance interface of LiverScan. Left B-mode, Right elastogram Source: [35]	10
2.9 In vivo assessment. Source: [35]	10
2.10 Measurement of HVRI using Doppler ultrasound. Source: [37]	11
2.11 Correlation of HVRI measurements with stages of Fibrosis Source: [37]	12
2.12 SVM model proposed in [43]	13
3.1 Relationship between AI, ML, NN and DL. Source:[51]	16
3.2 Examples for supervised and unsupervised learning. Source:[52]	17
3.3 Input, label and output of segmentation model. Source:[56] .	18
3.4 Architecture of Unet Model. Source: [54]	19
3.5 Convolution and Transposed Convolution with a 3X3 kernel and a stride of 1	21
3.6 Max Pool with 2x2 pool size. Source:[59]	21

3.7 Sigmoid Activation Function. Source:[60]	22
3.8 ReLU Activation Function. Source:[60]	23
3.9 ELU Activation Function with alpha=1. Source:[62]	24
3.10 Optical Flow Problem	25
3.11 Testing Optical Flow for a moving car	26
4.1 Block diagram of the method	30
4.2 Dataset preparation	32
4.3 VASA annotation tool	33
4.4 Learning curve of segmentation model	34
4.5 Model predictions	35
4.6 Region of excitation detection	36
4.7 Location of initial observers	37
4.8 Angle of movement of initial observers	39
4.9 Flow map of initial observer	39
4.10 Trajectories of movements in the liver	40
4.11 Initial and non-initial observers	41
4.12 Hypothesis visualization	42
4.13 Expected damping of trajectories in healthy liver (a) vs fibrotic liver (b)	42
4.14 Expected damping of magnitudes at various fibrosis stages .	43
5.1 Flow map of one observer and threshold values	46
5.2 Box plot of magnitudes for healthy liver (F0/F1)	47
5.3 Box plot of magnitudes for fibrotic liver (F4)	47
5.4 Observer placement and their damping of mean of magnitudes(1)	48
5.5 Trajectories and their damping of mean of magnitudes(2) . .	49
5.6 Observer placement and their damping of mean of magnitudes(3)	50

5.7 Damping of mean of magnitudes of fibrotic stages	51
5.8 Average damping of fibrosis stages	52
5.9 Box plot of stage wise damping values	52
7.1 Box plot of magnitudes for Pid_017	56
7.2 Possible observers for future analysis	56

C

List of Tables

2.1 Stages of fibrosis	4
4.1 Liver stiffness and fibrosis stages dataset	31
4.2 Standard cutoff values. Source: [70]	31
4.3 Hyperparameters for segmentation model	34
4.4 Parameters of optical flow API of OpenCV library [68]	38

D

Bibliography

- [1] Vikramjit Mitra and Jane Metcalf. Metabolic functions of the liver. *Anaesthesia & Intensive Care Medicine*, 13(2):54–55, 2012.
- [2] Elliot B Tapper and Neehar D Parikh. Mortality due to cirrhosis and liver cancer in the united states, 1999-2016: observational study. *bmj*, 362, 2018.
- [3] Jakob Manthey, Kevin D Shield, Margaret Rylett, Omer SM Hasan, Charlotte Probst, and Jürgen Rehm. Global alcohol exposure between 1990 and 2017 and forecasts until 2030: a modelling study. *The Lancet*, 393(10190):2493–2502, 2019.
- [4] Fuat Ozkan, Yasemin Coskun Yavuz, Mehmet Fatih Inci, Bulent Altunoluk, Nuri Ozcan, Murvet Yuksel, Hayriye Sayarlioglu, and Ekrem Dogan. Interobserver variability of ultrasound elastography in transplant kidneys: correlations with clinical-doppler parameters. *Ultrasound in medicine & biology*, 39(1):4–9, 2013.
- [5] Marie Byenfeldt, Anders Elvin, and Per Fransson. Influence of probe pressure on ultrasound-based shear wave elastography of the liver using comb-push 2-d technology. *Ultrasound in medicine & biology*, 45 (2):411–428, 2019.
- [6] Ramón Bataller, David A Brenner, et al. Liver fibrosis. *The Journal of clinical investigation*, 115(2):209–218, 2005.
- [7] Tsuyoshi Shiina, Tomonori Maki, Makoto Yamakawa, Tsuyoshi Mitake, Masatoshi Kudo, and Kenji Fujimoto. Mechanical model analysis for quantitative evaluation of liver fibrosis based on ultrasound

- tissue elasticity imaging. *Japanese Journal of Applied Physics*, 51(7S):07GF11, 2012.
- [8] RC Benyon and JP Iredale. Is liver fibrosis reversible? *Gut*, 46(4):443–446, 2000.
 - [9] Frank Tacke and Christian Trautwein. Mechanisms of liver fibrosis resolution. *Journal of hepatology*, 63(4):1038–1039, 2015.
 - [10] Delaram Eskandari, Niloofar Khodabandehloo, Hosein Samadani-fard, Amir Ziaeef, and Alireza Hejrati. A review of the available remedial procedures for the treatment of fatty liver disease. *Pak. J. Med. Health Sci.*, 14(2):1292–1300, 2020.
 - [11] Arturo A Bravo, Sunil G Sheth, and Sanjiv Chopra. Liver biopsy. *New England Journal of Medicine*, 344(7):495–500, 2001.
 - [12] Arie Regev, Mariana Berho, Lennox J Jeffers, Clara Milikowski, Enrique G Molina, Nikolaos T Pyrsopoulos, Zheng-Zhou Feng, K Rajender Reddy, and Eugene R Schiff. Sampling error and intraobserver variation in liver biopsy in patients with chronic hcv infection. *The American journal of gastroenterology*, 97(10):2614–2618, 2002.
 - [13] Christine H Janes and Keith D Lindor. Outcome of patients hospitalized for complications after outpatient liver biopsy. *Annals of Internal Medicine*, 118(2):96–98, 1993.
 - [14] Andrea Lut. Liver fibrosis: Patients can be at risk of death even without exhibiting symptoms. URL <https://www.siemens-healthineers.com/at/news/mso-liver-fibrosis>.
 - [15] William MC Rosenberg, Michael Voelker, Robert Thiel, Michael Becka, Alastair Burt, Detlef Schuppan, Stefan Hubscher, Tania Roskams, Massimo Pinzani, Michael JP Arthur, et al. Serum markers detect the presence of liver fibrosis: a cohort study. *Gastroenterology*, 127(6):1704–1713, 2004.
 - [16] Julie Parkes, Indra Neil Guha, Paul Roderick, and William Rosenberg. Performance of serum marker panels for liver fibrosis in chronic hepatitis c. *Journal of hepatology*, 44(3):462–474, 2006.

-
- [17] Mohammad S Siddiqui, Raj Vuppalanchi, Mark L Van Natta, Erin Hallinan, Kris V Kowdley, Manal Abdelmalek, Brent A Neuschwander-Tetri, Rohit Loomba, Srinivasan Dasarathy, Danielle Brandman, et al. Vibration-controlled transient elastography to assess fibrosis and steatosis in patients with nonalcoholic fatty liver disease. *Clinical Gastroenterology and Hepatology*, 17(1):156–163, 2019.
 - [18] Shear wave elastography. . URL <https://www.sciencedirect.com/topics/nursing-and-health-professions/shear-wave-elastography>.
 - [19] M Yoneda, H Mawatari, K Fujita, H Endo, H Iida, Y Nozaki, K Yonemitsu, T Higurashi, H Takahashi, N Kobayashi, et al. Noninvasive assessment of liver fibrosis by measurement of stiffness in patients with nonalcoholic fatty liver disease (nafld). *Digestive and Liver Disease*, 40(5):371–378, 2008.
 - [20] Nezam H Afdhal. Fibroscan (transient elastography) for the measurement of liver fibrosis. *Gastroenterology & hepatology*, 8(9):605, 2012.
 - [21] Julius Wilder M.D. Ph.D Keyur Patel M.D. Shear wave elastography. URL <https://aasldpubs.onlinelibrary.wiley.com/doi/pdf/10.1002/cld.407>.
 - [22] Atlantic Gastroenterology. Fibroscan liver elastography. URL <https://www.atgastro.com/fibroscan-brooklyn-ny/>.
 - [23] Fibroscan, liver elastography and cap scan for fatty liver disease or nash, . URL <http://gastroliverclinic.com.au/services/fibroscan-liver-elastography-cap-scan/>.
 - [24] G Sánchez Antolin, F Garcia Pajares, MA Vallecillo, P Fernandez Orcajo, S Gómez de la Cuesta, M Gonzalez Sagrado, R Velicia, and A Caro-Patón. Fibroscan evaluation of liver fibrosis in liver transplantation. 41(3):1044–1046, 2009.
 - [25] Umberto Arena, Monica Lupson Platon, Cristina Stasi, Stefania Moscarella, Alì Assarat, Giorgio Bedogni, Valeria Piazzolla, Radu Badea, Giacomo Laffi, Fabio Marra, et al. Liver stiffness is influenced by a standardized meal in patients with chronic hepatitis c virus at different stages of fibrotic evolution. *Hepatology*, 58(1):65–72, 2013.

-
- [26] Kento Imajo, Takaomi Kessoku, Yasushi Honda, Wataru Tomeno, Yuji Ogawa, Hironori Mawatari, Koji Fujita, Masato Yoneda, Masataka Taguri, Hideyuki Hyogo, et al. Magnetic resonance imaging more accurately classifies steatosis and fibrosis in patients with nonalcoholic fatty liver disease than transient elastography. *Gastroenterology*, 150(3):626–637, 2016.
 - [27] Siddharth Singh, Sudhakar K Venkatesh, Zhen Wang, Frank H Miller, Utaroh Motosugi, Russell N Low, Tarek Hassanein, Patrick Asbach, Edmund M Godfrey, Meng Yin, et al. Diagnostic performance of magnetic resonance elastography in staging liver fibrosis: a systematic review and meta-analysis of individual participant data. *Clinical Gastroenterology and Hepatology*, 13(3):440–451, 2015.
 - [28] Suraj D Serai, Nancy A Obuchowski, Sudhakar K Venkatesh, Claude B Sirlin, Frank H Miller, Edward Ashton, Patricia E Cole, and Richard L Ehman. Repeatability of mr elastography of liver: a meta-analysis. *Radiology*, 285(1):92–100, 2017.
 - [29] Tomohiro Takamura, Utaroh Motosugi, Shintaro Ichikawa, Katsuhiro Sano, Hiroyuki Morisaka, Tomoaki Ichikawa, Nobuyuki Enomoto, and Hiroshi Onishi. Usefulness of mr elastography for detecting clinical progression of cirrhosis from child-pugh class a to b in patients with type c viral hepatitis. *Journal of Magnetic Resonance Imaging*, 44(3):715–722, 2016.
 - [30] M Stoopen-Rometti, ER Encinas-Escobar, CR Ramirez-Carmona, E Wolpert-Barraza, E Kimura-Hayama, LA Sosa-Lozano, R Favila, Y Kimura-Fujikami, JA Saavedra-Abril, and A Loaeza-del Castillo. Diagnosis and quantification of fibrosis, steatosis, and hepatic siderosis through multiparametric magnetic resonance imaging. *Revista de Gastroenterología de México (English Edition)*, 82(1):32–45, 2017.
 - [31] Mireen Friedrich-Rust, Mei-Fang Ong, Swantje Martens, Christoph Sarrazin, Joerg Bojunga, Stefan Zeuzem, and Eva Herrmann. Performance of transient elastography for the staging of liver fibrosis: a meta-analysis. *Gastroenterology*, 134(4):960–974, 2008.
 - [32] Gerald Kircheis, Abdurrahman Sagir, Christoph Vogt, Stephan Vom Dahl, Ralf Kubitz, and Dieter Häussinger. Evaluation of acoustic

- radiation force impulse imaging for determination of liver stiffness using transient elastography as a reference. *World Journal of Gastroenterology: WJG*, 18(10):1077, 2012.
- [33] Éric Bavu, Jean-Luc Gennisson, Mathieu Couade, Jeremy Bercoff, Vincent Mallet, Mathias Fink, Anne Badel, Anaïs Vallet-Pichard, Bertrand Nalpas, Mickaël Tanter, et al. Noninvasive in vivo liver fibrosis evaluation using supersonic shear imaging: a clinical study on 113 hepatitis c virus patients. *Ultrasound in medicine & biology*, 37(9):1361–1373, 2011.
 - [34] Antonio Orlacchio, Francesca Bolacchi, Marco Antonicoli, Irene Coco, Elisa Costanzo, Daniela Tosti, Simona Franciosi, Mario Angelico, and Giovanni Simonetti. Liver elasticity in nash patients evaluated with real-time elastography (rte). *Ultrasound in medicine & biology*, 38(4):537–544, 2012.
 - [35] Tak-Man Mak, Yan-Ping Huang, and Yong-Ping Zheng. Liver fibrosis assessment using transient elastography guided with real-time b-mode ultrasound imaging: a feasibility study. *Ultrasound in medicine & biology*, 39(6):956–966, 2013.
 - [36] Christophe Aubé, Betsy Winkfield, Frédéric Oberti, Eric Vuillemin, Marie C Rousselet, Christine Caron, and Paul Calès. New doppler ultrasound signs improve the non-invasive diagnosis of cirrhosis or severe liver fibrosis. *European journal of gastroenterology & hepatology*, 16(8):743–751, 2004.
 - [37] HH Lutz, N Gassler, FW Tischendorf, C Trautwein, and JJW Tischendorf. Doppler ultrasound of hepatic blood flow for noninvasive evaluation of liver fibrosis compared with liver biopsy and transient elastography. *Digestive diseases and sciences*, 57(8):2222–2230, 2012.
 - [38] Rabia Ergelen, Yusuf Yilmaz, Ruslan Asedov, Cigdem Celikel, Hakan Akin, Onur Bugdayci, Ersan Altun, and Davut Tuney. Comparison of doppler ultrasound and transient elastography in the diagnosis of significant fibrosis in patients with nonalcoholic steatohepatitis. *Abdominal Radiology*, 41(8):1505–1510, 2016.
 - [39] HH Lutz, B Schroeter, DC Kroy, U Neumann, C Trautwein, and JJW Tischendorf. Doppler ultrasound and transient elastography in liver

- transplant patients for noninvasive evaluation of liver fibrosis in comparison with histology: a prospective observational study. *Digestive diseases and sciences*, 60(9):2825–2831, 2015.
- [40] A Colli, M Cocciole, C Riva, E Martinez, A Prisco, M Pirola, and G Bratina. Abnormalities of doppler waveform of the hepatic veins in patients with chronic liver disease: correlation with histologic findings. *AJR. American journal of roentgenology*, 162(4):833–837, 1994.
 - [41] Alexandra von Herbay, Thomas Frieling, and Dieter Häussinger. Association between duplex doppler sonographic flow pattern in right hepatic vein and various liver diseases. *Journal of clinical ultrasound*, 29(1):25–30, 2001.
 - [42] Thomas Bernatik, Deike Strobel, Eckhart Georg Hahn, and Dirk Becker. Doppler measurements: a surrogate marker of liver fibrosis? *European journal of gastroenterology & hepatology*, 14(4):383–387, 2002.
 - [43] Lili He, Hailong Li, Jonathan A Dudley, Thomas C Maloney, Samuel L Brady, Elanchezhian Somasundaram, Andrew T Trout, and Jonathan R Dillman. Machine learning prediction of liver stiffness using clinical and t2-weighted mri radiomic data. *American Journal of Roentgenology*, 213(3):592–601, 2019.
 - [44] Corinna Cortes and Vladimir Vapnik. Support-vector networks. *Machine learning*, 20(3):273–297, 1995.
 - [45] H He, Y Bai, EA Garcia, and S ADASYN Li. adaptive synthetic sampling approach for imbalanced learning. *ieee international joint conference on neural networks*. 2008.
 - [46] Somaya Hashem, Gamal Esmat, Wafaa Elakel, Shahira Habashy, Safaa Abdel Raouf, Mohamed Elhefnawi, Mohamed I Eladawy, and Mahmoud ElHefnawi. Comparison of machine learning approaches for prediction of advanced liver fibrosis in chronic hepatitis c patients. *IEEE/ACM transactions on computational biology and bioinformatics*, 15(3):861–868, 2017.
 - [47] Khoschy Schawkat, Alexander Ciritsis, Sophie von Ulmenstein, Hanna Honcharova-Biletska, Christoph Jüngst, Achim Weber,

- Christoph Gubler, Joachim Mertens, and Caecilia S Reiner. Diagnostic accuracy of texture analysis and machine learning for quantification of liver fibrosis in mri: correlation with mr elastography and histopathology. *European radiology*, 30(8):4675–4685, 2020.
- [48] Hiroki Kato, Masayuki Kanematsu, Xuejun Zhang, Masanao Saio, Hiroshi Kondo, Satoshi Goshima, and Hiroshi Fujita. Computer-aided diagnosis of hepatic fibrosis: preliminary evaluation of mri texture analysis using the finite difference method and an artificial neural network. *American Journal of Roentgenology*, 189(1):117–122, 2007.
- [49] Michael J House, Sander J Bangma, Mervyn Thomas, Eng K Gan, Oyekoya T Ayonrinde, Leon A Adams, John K Olynyk, and Tim G St. Pierre. Texture-based classification of liver fibrosis using mri. *Journal of Magnetic Resonance Imaging*, 41(2):322–328, 2015.
- [50] HeiShun Yu, Karen Buch, Baojun Li, Michael O’Brien, Jorge Soto, Hernan Jara, and Stephan W Anderson. Utility of texture analysis for quantifying hepatic fibrosis on proton density mri. *Journal of Magnetic Resonance Imaging*, 42(5):1259–1265, 2015.
- [51] Yulia Gavrilova. Ai vs ml vs dl: Essentials. URL <https://serokell.io/blog/ai-ml-dl-difference>.
- [52] Supervised learning vs unsupervised learning. URL <https://lawtomated.com/supervised-vs-unsupervised-learning-which-is-better>.
- [53] Selim Seferbekov, Vladimir Iglovikov, Alexander Buslaev, and Alexey Shvets. Feature pyramid network for multi-class land segmentation. pages 272–275, 2018.
- [54] Olaf Ronneberger, Philipp Fischer, and Thomas Brox. U-net: Convolutional networks for biomedical image segmentation. pages 234–241, 2015.
- [55] Jonathan Long, Evan Shelhamer, and Trevor Darrell. Fully convolutional networks for semantic segmentation. pages 3431–3440, 2015.

-
- [56] Manpreet Singh Minhas. Transfer learning for segmentation. URL <https://towardsdatascience.com/transfer-learning-for-segmentation-using-deeplabv3-in-pytorch-f770863d>
 - [57] Vijay Badrinarayanan, Alex Kendall, and Roberto Cipolla. Segnet: A deep convolutional encoder-decoder architecture for image segmentation. *IEEE transactions on pattern analysis and machine intelligence*, 39(12):2481–2495, 2017.
 - [58] Guosheng Lin, Anton Milan, Chunhua Shen, and Ian Reid. Refinenet: Multi-path refinement networks for high-resolution semantic segmentation. pages 1925–1934, 2017.
 - [59] Max-pooling, . URL https://computersciencewiki.org/index.php/Max-pooling_-_Pooling.
 - [60] Activation function - sigmoid, tanh and relu, . URL <https://www.programmersought.com/article/2203107446/>.
 - [61] Djork-Arné Clevert, Thomas Unterthiner, and Sepp Hochreiter. Fast and accurate deep network learning by exponential linear units (elus). *arXiv preprint arXiv:1511.07289*, 2015.
 - [62] Danqing Liu. A practical guide to relu. URL <https://medium.com/@danqing/a-practical-guide-to-relu-b83ca804f1f7>.
 - [63] Massimo Tistarelli, Francesco Guarinotta, Danilo Rizzieri, and Federico Tarocchi. Application of optical flow for automated overtaking control. pages 105–112, 1994.
 - [64] W Kruger, Wirfried Enkelmann, and S Rossle. Real-time estimation and tracking of optical flow vectors for obstacle detection. pages 304–309, 1995.
 - [65] Loren Arthur Schwarz, Artashes Mkhitaryan, Diana Mateus, and Nasir Navab. Human skeleton tracking from depth data using geodesic distances and optical flow. *Image and Vision Computing*, 30(3):217–226, 2012.
 - [66] Andreas Ranftl, Fernando Alonso-Fernandez, and Stefan Karlsson. Face tracking using optical flow. pages 1–5, 2015.

-
- [67] Konstantinos G Derpanis. The harris corner detector. *York University*, 2, 2004.
 - [68] G. Bradski. The OpenCV Library, 2000.
 - [69] Seung Up Kim, Gi Hong Choi, Woong Kyu Han, Beom Kyung Kim, Jun Yong Park, Do Young Kim, Jin Sub Choi, Seung Choul Yang, Eun Hee Choi, Sang Hoon Ahn, et al. What are ‘true normal’liver stiffness values using fibroscan®?: a prospective study in healthy living liver and kidney donors in south korea. *Liver International*, 30(2):268–274, 2010.
 - [70] Shear wave elastography, . URL https://www.uhn.ca/PatientsFamilies/Health_information/Health_Topics/Documents/FibroScan_Liver_Disease.pdf.
 - [71] E. Coto, A. Dutta, and A. Zisserman. VGG annotation search and annotator (VASA). <http://www.robots.ox.ac.uk/~vgg/software/vasa/>, 2020.
 - [72] Francois Chollet et al. Keras, 2015. URL <https://github.com/fchollet/keras>.
 - [73] Martín Abadi, Ashish Agarwal, Paul Barham, Eugene Brevdo, Zhifeng Chen, Craig Citro, Greg S. Corrado, Andy Davis, Jeffrey Dean, Matthieu Devin, Sanjay Ghemawat, Ian Goodfellow, Andrew Harp, Geoffrey Irving, Michael Isard, Yangqing Jia, Rafal Jozefowicz, Lukasz Kaiser, Manjunath Kudlur, Josh Levenberg, Dandelion Mané, Rajat Monga, Sherry Moore, Derek Murray, Chris Olah, Mike Schuster, Jonathon Shlens, Benoit Steiner, Ilya Sutskever, Kunal Talwar, Paul Tucker, Vincent Vanhoucke, Vijay Vasudevan, Fernanda Viégas, Oriol Vinyals, Pete Warden, Martin Wattenberg, Martin Wicke, Yuan Yu, and Xiaoqiang Zheng. TensorFlow: Large-scale machine learning on heterogeneous systems, 2015. URL <https://www.tensorflow.org/>. Software available from tensorflow.org.
 - [74] Kaiming He, Xiangyu Zhang, Shaoqing Ren, and Jian Sun. Delving deep into rectifiers: Surpassing human-level performance on imagenet classification. pages 1026–1034, 2015.

- [75] Seyed Sadegh Mohseni Salehi, Deniz Erdogmus, and Ali Gholipour. Tversky loss function for image segmentation using 3d fully convolutional deep networks. pages 379–387, 2017.
- [76] Pauli Virtanen, Ralf Gommers, Travis E. Oliphant, Matt Haberland, Tyler Reddy, David Cournapeau, Evgeni Burovski, Pearu Peterson, Warren Weckesser, Jonathan Bright, Stéfan J. van der Walt, Matthew Brett, Joshua Wilson, K. Jarrod Millman, Nikolay Mayorov, Andrew R. J. Nelson, Eric Jones, Robert Kern, Eric Larson, C J Carey, İlhan Polat, Yu Feng, Eric W. Moore, Jake VanderPlas, Denis Laxalde, Josef Perktold, Robert Cimrman, Ian Henriksen, E. A. Quintero, Charles R. Harris, Anne M. Archibald, Antônio H. Ribeiro, Fabian Pedregosa, Paul van Mulbregt, and SciPy 1.0 Contributors. SciPy 1.0: Fundamental Algorithms for Scientific Computing in Python, 2020.
- [77] John Canny. A computational approach to edge detection. *IEEE Transactions on pattern analysis and machine intelligence*, (6):679–698, 1986.
- [78] Wen-Chun Yeh, Pai-Chi Li, Yung-Ming Jeng, Hey-Chi Hsu, Po-Ling Kuo, Meng-Lin Li, Pei-Ming Yang, and Po Huang Lee. Elastic modulus measurements of human liver and correlation with pathology. *Ultrasound in medicine & biology*, 28(4):467–474, 2002.
- [79] Thomas A Wynn. Cellular and molecular mechanisms of fibrosis. *The Journal of Pathology: A Journal of the Pathological Society of Great Britain and Ireland*, 214(2):199–210, 2008.

Declaration of Academic Integrity

I hereby declare that I have written the present work myself and did not use any sources or tools other than the ones indicated.

Date:
(Signature)